



Contents lists available at ScienceDirect

Journal of Quantitative Spectroscopy & Radiative Transfer

journal homepage: www.elsevier.com/locate/jqsrt



K_α resonance fluorescence in Al, Ti, Cu and potential applications for X-ray sources



Sultana N. Nahar, Anil K. Pradhan

Department of Astronomy, The Ohio State University, Columbus, OH 43210, USA

ARTICLE INFO

Article history:

Received 11 July 2014

Received in revised form

13 October 2014

Accepted 16 October 2014

Available online 14 November 2014

Keywords:

K_α transitions in Al

Ti and Cu ions

X-ray fluorescence effects

Absorption coefficients

X-rays source

ABSTRACT

The K_α resonance fluorescence (RFL) effect via photoabsorptions of inner shell electrons as the element goes through multiple ionization states is studied. We demonstrate that the resonances observed recently in K_α (1s-2p) fluorescence in aluminum plasmas by using a high-intensity X-ray free-electron laser [1] are basically K-shell resonances in hollow atoms going through multiple ionization states at resonant energies as predicted earlier for gold and iron ions [2]. These resonances are formed below the K-shell ionization edge and shift toward higher energies with ionization states, as observed. Fluorescence emission intensities depend on transition probabilities for each ionization stage of the given element for all possible K_α (1s→2p) transition arrays. The present calculations for resonant photoabsorptions of K_α photons in Al have reproduced experimentally observed features. Resonant cross sections and absorption coefficients are presented for possible observation of K_α RFL in the resonant energy ranges of 4.5–5.0 keV for Ti ions and 8.0–8.7 keV for Cu ions respectively. We suggest that theoretically the K_α RFL process may be driven to enhance the Auger cycle by a twin-beam monochromatic X-ray source, tuned to the K-edge and K_α energies, with potential applications such as the development of narrow-band biomedical X-ray devices.

© 2014 Elsevier Ltd. All rights reserved.

1. Introduction

Excitation of resonances in atoms with inner-shell vacancies has been under considerable theoretical and experimental study recently (e.g. [1–6]). In addition to basic phenomena of intrinsic physical interest, there are two main reasons for these studies: the potential for novel practical applications, such as in biomedicine [3], and the advent of high-intensity radiation or electron sources, such as the X-ray free-electron laser (XFEL) [7], required to create a high-energy-density (HED) [8] plasma containing

the “hollow” atomic ions. The experiment by Vinko et al. [1] used the Linac Coherent Light Source (LCLS) XFEL at the Stanford Linear Accelerator (SLAC) to create a solid-density aluminum plasma, where several ionization states can exist with K-shell vacancies. When the XFEL energy equaled the K_α energy for the 1s-2p transition, resonant fluorescence (RFL) was initiated and manifested itself as K_α emission which was observed. RFL was found to occur below the K-shell ionization edge created in double-core-excited hollow ions [7,6], sometimes referred to as “hidden” resonances [5]. Experimental diagnostics centered on K_α resonant fluorescence: K-shell ionization was followed by K_α emission with an l→K transition creating a vacancy in the L-shell. RFL was then triggered by resonant K→L excitation by XFEL. A theoretical description of K_α RFL requires an elaborate treatment.

E-mail address: nahar.1@osu.edu (S.N. Nahar).
URL: <http://www.astronomy.ohio-state.edu/~nahar> (S.N. Nahar).

In previous works, K_{α} resonance complexes were studied with a view towards observations from X-ray astronomical observatories, viz. *Chandra*, *X-ray Multi-Mirror Mission*, *Suzaku*. For example, we considered X-ray absorption via K_{α} resonance complexes in oxygen [9]. However, the K_{α} analysis of laboratory experiments is more problematic owing to their transient nature and different temperature-density regimes. Unlike astrophysical observations that seek to model absorption along line-of-sight in optically thin sources, the *in situ* laboratory measurements entail not only absorption but K_{α} emission that would entail all possible processes and transitions contributing to Auger decays. A more extensive computational methodology and relevant atomic data are required to model K_{α} RFL in intense X-ray sources.

Our earlier theoretical calculations for transition probabilities and cross sections of several high Z elements, such as Au, Pt, Pb, W, U, etc., were carried out for all ionization states that can possibly be involved in K_{α} excitations, from H-like to F-like ionization stages [10,11,4,12,13], and for all resonances from K_{α} to K_{η} , i.e. K→L, M, N, O, P in gold and iron [2]. Similar work, but for the radiative and Auger decay rates and widths instead of absorption cross sections, for K_{α} transitions of the elements of present interest, has been reported by Palmeri et al. [14,15]. They used the semi-empirical Cowan's code, incorporating the Hartree-Fock method with relativistic corrections, for Al K lines [14], and K lines of iron peak and light odd-Z elements [15]. In this work we report the K_{α} transitions obtained using relativistic Breit-Pauli approximation implemented in SUPERSTRUCTURE code [16,17] and extend the calculations to establish a correspondence between the observed K_{α} resonances in Al ions [1] and the computed resonant absorption (Fig. 2, Ref. [2]). We also present resonant energies and strengths for titanium and copper for comparison with future laboratory observations using intense plasma X-ray sources and HED plasmas. These elements are under proposed investigation due to their ready availability and excitation by X-rays of lower energy than other heavier elements.

While X-ray sources such as synchrotron [18,19] and now XFEL are monochromatic and capable of high fluence that enables new experimentation, they are not readily available or suitable for technological or biomedical use. Whereas the task of creating deep inner-shell holes remains daunting in ordinary situations, it is worth exploring what might be the least energetic requirement to pump RFL efficiently. In this report we propose a schematic twin-beam monochromatic X-ray set up. This might enable applications such as localized X-ray deposition in high-Z radiosensitization in radiation therapy (e.g. [3]). Recent theoretical studies have shown that relatively low energy X-rays in the $E < 100$ keV range should be far more effective than the conventional high energy X-rays in the MeV range generated by linear accelerators (LINACs) used in radiation therapy (e.g. [20–24]). Monochromatic X-ray systems, if available, should be ideal for irradiation. Potential applications of monochromatic X-ray systems have been proposed in biomedical spectroscopy for imaging and therapy. Tuned to a spectroscopic energy, such as the K-edge, these X-rays upon irradiation may breakdown

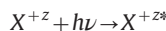
high-Z compounds of platinum or gold in nanomoties delivered to tumors, via Auger decays resulting in low-energy-transfer (LET) electrons (e.g. [3,18,19,25–27]).

2. Theory

Atomic processes and calculations for the positions and strengths of K_{α} resonances, and corresponding Auger decay mechanism, are briefly described in two subsections. A theoretical model for driving K_{α} resonances and the Auger cycle using a twin-beam set-up of two monochromatic X-ray beams is presented in a separate subsection.

2.1. K_{α} resonances

The two radiative processes that occur due to X-ray absorption by an element are photoexcitation and photoionization. In photoexcitation an electron is excited to a higher energy level



where the asterisk (*) denotes an excited state. Its strength is determined by the oscillator strength (f) while the de-excitation is determined by the radiative decay rate or Einsteins A-coefficient. In photoionization an electron is energetic enough to be free, that is, to go to continuum



This direct ionization gives the background feature of the process. Photoionization also occurs via an intermediate doubly excited autoionizing state as described below. An electron collides with an ion and forms a doubly excited (double asterisks) autoionizing state

$$e + X^{+z} \rightleftharpoons (X^{+z-1})^{**} \rightleftharpoons \begin{cases} e + X^{+z} & AI \\ X^{+z-1} + h\nu & DR \end{cases}$$

The autoionizing state leads either to autoionization (AI) when the electron goes free or dielectronic recombination (DR) when a photon is emitted as the electron combines with the ion. The inverse of DR is photoionization. The autoionization state introduces a resonance in the process and has the most important impact on the ionization probability. The features in photoionization with energy are illustrated in the cross section σ_{pi} .

The oscillator strengths and photoionization cross sections can be obtained from the generalized line strengths as (e.g. [28])

$$S = \left| \left\langle \Psi_f \left| \sum_{j=1}^N r_j \right| \Psi_i \right\rangle \right|^2. \quad (1)$$

where Ψ_i and Ψ_f are the initial final state wave functions and the sum is over the number of electrons in the atomic system. For oscillator strengths (f_{ij}), the final wave function is bound while for photoionization cross sections (σ_{pi}), it is a continuum. f_{ij} , σ_{pi} and the mass attenuation coefficients κ can be obtained from generalized line strength as

$$f_{ij} = \left[\frac{E_{ji}}{3g_i} \right] S, \quad A_{ji} (\text{s}^{-1}) = \left[0.8032 \times 10^{10} \frac{E_{ji}^3}{3g_j} \right] S,$$

$$\sigma_{Pl}(k_\alpha, \nu) = 4\pi^2 \alpha \frac{E_{ij}}{3g_i} S a_o^2 = 8.064 \frac{E_{ij}}{3g_i} S [\text{Mb}],$$

$$\kappa(\nu; k_\alpha) = \frac{\sigma_{Pl}(\nu; k_\alpha)}{u W_A}. \quad (2)$$

where u is 1 amu = 1.66054×10^{-24} g and W_A is the atomic weight. Photoabsorption also depends on the ionization fractions of the element. Taking account of the ionization fractions for K- and L-shell ions, the attenuation coefficient is given by

$$\kappa(\nu; k_\alpha) = \frac{\sum_j w_j \sum_i \sigma_{Pl}(\nu; K - L_{ji}) / u A}{\sum_j w_j} \quad (3)$$

with w_j as the ionization fraction for an ion core j in the L-shell.

In a hollow atom, excitation by an electron to an upper vacant orbital appears as a resonance below its ionization energy. We demonstrated these resonances due to K-shell electron excitations to vacant L-, M-, N-, O-, P-shells forming below the K-shell ionization threshold in photoionization of gold and iron ions and computed the resonance energies and strengths for all ionization stages [2]. These resonances are directly related to K_α fluorescence effect.

For the resonant energies of K_α transitions, strengths and absorption coefficients of Al, Ti, and Cu ions, we carried out relativistic Breit–Pauli atomic structure calculations using the later version [17] of the atomic structure code SUPERSTRUCTURE [16] and extending an existing code PRCSS (e.g. [4]).

2.2. Auger decays and resonant absorption

Occurrence of resonant fluorescence (RFL) effect can be explained as follows. X-rays with energies higher than K-shell ionization energy of an element can photoionize it with creation of a hole in the K-shell. As shown in Fig. 1(i) [28], the hole is filled up by dropping of a L-shell electron when the excess energy of the electron is emitted as a photon. In a RFL condition, the emitted photon can knock out another L-shell electron which results in two holes in the L-shell. The two vacancies in the L-shell are then filled by two M-shell electrons creating four possible holes in

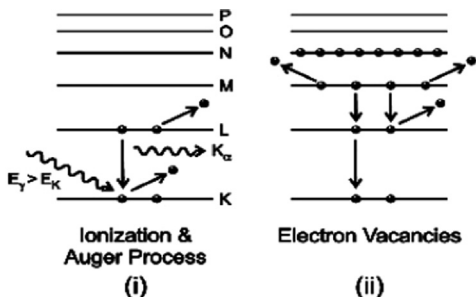


Fig. 1. K-shell photoionization and L \rightarrow K transition initiates Auger processes that result in multiple electron ejections via inter-subshell and intra-subshell transitions (Coster-Kronig and Super-Coster-Kronig and intra-subshell transitions (Coster-Kronig and Super-Coster-Kronig transitions respectively), as electron vacancies propagate up to higher (sub)shells.

the M-shell as in Fig. 1(ii). The process can lead to a cascade of electron and photon emissions, known as Coster–Kronig or Super-Coster–Kronig cascade, as multiple vacancies move upward through multiple ionization. Hence a single ionization of 1s electron can lead to ejection of 20 or more electrons in an ion with occupied O and P shells. However, to create the RFL condition, it is necessary for the element to have continuous absorption of K_α photons for K to L shell excitation as L-shell electrons drop to fill out the vacancies in the K-shell. The resonant channels become energetically accessible following K-shell ionization and Auger decays that open up multiple electronic vacancies in higher shells, particularly in high-Z atoms such as iron, platinum and gold [2,12].

For any two-level system $i \leftrightarrow j$ and transition frequency ν , the incident photon flux Φ at the resonant energy of K_α should be greater than the critical flux [2]

$$\Phi^c(\nu_{K_\alpha}) = \frac{\sum n_i > 2g_i A[n_i(S_i L_j i) \rightarrow 2(SLj)]}{g_K B_{K_\alpha}}. \quad (4)$$

where $n_i(S_i L_j i)$ refers to specific fine structure levels of an n -shell, e.g. 2($S_i L_j i$) refers to the L-shell levels. g_i and g_K are the statistical weight factors of the excited i th and K-shell, and B is the coefficient of photon absorption.

2.3. Twin-beam driven K_α resonance cycle

Whereas high intensity X-ray sources have now been shown to pump K_α RFL, a low intensity monochromatic X-ray source may not contain sufficient fluence to be effective in creating and pumping K_α RFL for useful purposes. In particular, monochromatic X-ray biomedical imaging and therapeutics would need to have far less intense fluxes in order to avoid damaging levels of radiation. One may therefore ask the question (albeit theoretically): what is the minimum intensity of an X-ray beam, or a combination of X-ray beams, that can be employed in principle to excite or pump K_α RFL?

As suggested in Montenegro et al. [3,29], one possibility to minimize the incident flux required for K_α RFL is a twin-beam monochromatic X-ray device. An external source with energy equal to K-L transition can be introduced to compete with the downward decays. Then the resonant excitation from the K-shell into electron vacancies in higher L-shell can result in RFL and increment in ejection of electrons. We explain the method schematically in Fig. 2. The two beams are tuned to the K-edge and the K_α resonance energies. K-shell ionization induced by the first beam would lead to electron vacancies in the L and higher shells via Auger decays. The second beam would pump the RFL mechanism, as well as cause secondary ionization from the emitted photon and electron ejections. The excitation/ionization processes are coupled and dependent on photon fluences of the two beams. Ultra fast monochromatic X-ray sources, such as the ones based on femtosecond PW lasers, would be suitable for the twin-beam configuration. A generalization of the proposed embodiment in Fig. 2, utilizing multiple monochromatic X-ray beams, may also be implemented. Such an extended system could target higher than K_α resonance complexes, as discussed in Pradhan et al. [2].

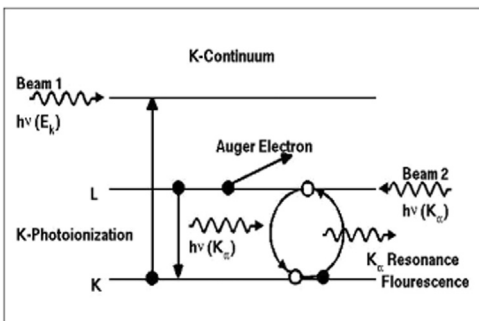


Fig. 2. Schematic diagram of a twin-beam monochromatic X-ray system. K-shell ionization by Beam I (on the left) with energies $h\nu \geq E_k$ triggers photon emission and Auger-electron cascades. Beam II containing K_α photons (on the right) drives resonant K_α fluorescence by pumping 1s electrons to 2p orbital.

A theoretical model for K_α RFL driven by two monochromatic X-ray beams is needed. That is necessary in order to develop a numerical collisional-radiative algorithm to simulate the physical processes illustrated in Fig. 2. The model employs atomic rates for excitation, ionization, photon fluences Φ_K , $\Phi_{K\alpha}$ in beams I and II respectively, K and L level

$$\Phi_{K\alpha}^e = \left\{ \frac{[\Phi_{K\alpha}^2 \sigma_{K\alpha}^R \sigma_L(E_K) N_L + \Phi_K \Phi_{K\alpha} \sigma_{K\alpha}^R (\sigma_L(E_K) N_L + \sigma_K(E_K) N_K \langle A_{LK^-} \rangle)]}{\sum_{n>2} \langle A_{nl^-} \rangle} + \Phi_K \sigma_K(E_K) N_K \right\} \frac{\omega_K \langle A_{LK^-} \rangle}{4\pi}. \quad (9)$$

populations, cascade coefficients from upper shells, etc. For instance, the L-shell population for each ion is governed by direct photoionizations by the two beams with Φ_1 and Φ_2 , collisional ionizations by electrons in the plasma at local density and temperature, cascades from outer shells, resonant excitation from the K-shell as well as stimulated emission $L \rightarrow K$ that constitutes the Auger cycle.

We proceed by writing down the rate equations for level populations determined by the two beams: Beam I with photon fluence Φ_K tuned to the K-shell ionization energy, and Beam II with fluence $\Phi_{K\alpha}$ tuned to the K_α resonance energy. However, since there are a large number of levels and symmetries involved, we simplify the notation, without loss of generality, in terms of populations and transition rates averaged over detailed level structure and corresponding transitions between allowed symmetries. We denote the level populations with a single-electron vacancy in the K and L shells as N_{K^-} and N_{L^-} respectively. Since L-shell ionization may be due to beams at both energies, we consider the L-level population separately. For Beam I tuned to the K-edge E_K , the L-shell population is

$$N_{L^-}^I \sum_{n>2} \langle A_{nl^-} \rangle = \Phi_K \sigma_L(E_K) N_L + \Phi_K \sigma_K(E_K) N_K \langle A_{LK^-} \rangle : Beam I, \quad (5)$$

so that

$$N_{L^-}^I = \frac{\Phi_K [\sigma_L(E_K) N_L + \sigma_K(E_K) N_K \langle A_{LK^-} \rangle]}{\sum_{n>2} \langle A_{nl^-} \rangle} : Beam I, \quad (6)$$

where $\langle A_{nl^-} \rangle$ and $\langle A_{LK^-} \rangle$ are the averaged A -values over all possible transitions filling the L-shell and K-shell single-electron vacancies, and $\sigma(E_K)$ is the photoionization cross section at the K-edge. Now consider L-shell population due to ionizations by Beam II, tuned to K_α energy $E(K_\alpha)$, and radiative decays from higher levels

$$N_{L^-}^H \sum_{n>2} \langle A_{nl^-} \rangle = \Phi_{K\alpha} \sigma_L(E_{K\alpha}) N_L : Beam II. \quad (7)$$

L-shell vacancies are an *a priori* requirement to drive K_α RFL. Given these vacancies, the rate of K_α absorption from Beam II tuned to K_α energy would drive the RFL cycle, and the resulting K_α emission would indicate its strength. While absorption from the two incident beams is unidirectional, emission is generally isotropic. The fluorescence yield for $L \rightarrow K$ transitions for high-Z atoms approaches unity, $\omega_K(Z) \rightarrow 1$. Laboratory experiments measure K_α emission from the dominant ionization states of an element. The rate equations for the emitted K_α fluence $\Phi_{K\alpha}^e$ then depends on K-shell ionizations and resonant absorption cross section $\sigma_{K\alpha}^R$ as follows:

$$\Phi_{K\alpha}^e = \frac{\omega_K}{4\pi} [\Phi_K \sigma_K(E_K) N_K + (N_L^I + N_L^H) \sigma_{K\alpha}^R \Phi_{K\alpha}] \langle A_{LK^-} \rangle. \quad (8)$$

Using Eqs. (6) and (7), the emitted K_α fluence from the RFL cycle driven by the two beams is

The K_α RFL is driven by coupling of unidirectional beams tuned to the K-edge and the K_α energies. Eq. (9) is non-linear in incident beam fluence $\Phi_{K\alpha}$; the multiplicative factors comprising of the resonant cross section $\sigma_{K\alpha}^R$ and $\sigma_L(E_K)$ are small. So while the emitted K_α intensity in the K_α RFL cycle may increase non-linearly, the K_α flux would be small unless the two beams driving RFL are extremely intense. Such a situation is clearly achievable in the LCLS experiments, even with a single XFEL. It may also be possible in synchrotron if the primary beam can be split up into two at the K-edge and the K_α energies.

Given the photon fluences in the two beams, we may obtain an estimate of induced Rabi oscillations at frequency $\Omega_R = \mu_{KL} E / \hbar$, where μ_{KL} is the dipole moment related to the A -coefficient for a given $K \rightarrow L$ transition, and E is the electric field amplitude corresponding to the radiance (time-averaged power per unit area) $I = \frac{1}{2} c \epsilon_0 E^2$ in Beam II with fluence $\Phi_{K\alpha}^2$. Though complex, such a model is computationally feasible. However, the primary requirement is the calculation of the cross sections, transition probabilities, and rates for all contributing processes mentioned above. The development of an algorithm and a computational framework will be the subject of subsequent works. In this paper we present the two-beam RFL concept, theoretical expressions, correspondence with experimental measurements, and the type of atomic calculations needed for their evaluation. Preliminary order-of-magnitude estimates are presented in the next section.

3. Results and discussion

In order to facilitate a correspondence with K_{α} RFL measurements, we have computed the K_{α} resonant absorption attenuation coefficients (cm^2/g). In earlier theoretical investigations of K-shell resonances [2,3] we showed that the cross sections for resonant photoexcitations of K_{α} , K_{β} , etc., forming below the K-shell ionization edge, are orders of magnitude higher than the photoionization background for high Z elements, such as gold ($Z=79$). Being much lower in Z (13), aluminum will have lower resonant peaks compared to the background, but can be visible as manifested in the experiment [1].

A quantitative description of averaged energies and K_{α} resonance strengths is given in Table 1 for H- to F-like ionization states for aluminum. The number of transitions, and relative positions and K_{α} strengths, can be discerned readily from the averaged fine structure energies and cross sections σ_{pi} (megabarns) derived from resonance oscillator strengths. The number of transitions between the two orbitals, 1s and 2p, can change significantly depending on the number of electrons in the orbitals. Inclusion of fine structure plays a role in the number. For example, there are a large number of K_{α} transitions that come into play, such as 35 for C- and N-like ionization stages, whereas it is 2 for He- and Be-like ions. A total of 112 transitions are allowed quantum mechanically for all H- to F-like ions [10]. The number is larger if forbidden transitions are included. However, the strength and oscillator strengths are much weaker than that of allowed transitions. The absorption coefficients for various ionization stages vary from 10^4 to $10^5 \text{ cm}^2/\text{g}$ whereas the background coefficient is of the order of $10^2 \text{ cm}^2/\text{g}$ [30]. The resonant peaks are even higher than the K-edge peak of about $4 \times 10^3 \text{ Mb}$ as given in NIST website [30]. Table 2 gives the energies, oscillator strengths, A -values, line strengths for individual transitions. These and all atomic data from the structure calculations will be available electronically at the on-line database NORAD-Atomic-Data [31].

The averaged energy positions of various ionization stages, He-like to F-like aluminum ions, are specified in Fig. 3 (pointed by arrows). However, the peak positions seen are due to fine structure components. The number of electron emissions depends on the radiative decay rates

or Einstein's A -coefficients and hence there may be more of one ionization stage than the others giving variation in peaks. Typically K-L (K_{α}) transitions have the highest probabilities or A -values and show as high peak resonances in the photoionization cross sections. Many of the resonances of multiple ionization stages overlap among adjacent ionization stages. These need to be taken into account for the overall spectrum. The resulting K_{α} absorption that drives RFL pumping is shown in top panel of Fig. 3 and compared with the experimental spectrum (lower panel) [1]. The cross sections used to compute the resonance structures in Fig. 3 were convolved with a small Gaussian beam width of 10 eV FWHM. Evidently, the K_{α} absorption resonance complexes for each ion can be associated with the K_{α} emission seen experimentally (lower panel). The rising trend in relative intensities, measured as “Emitted photon number ($\text{sr}^{-1}\text{eV}^{-1}$)” [1,2], is also evident in the theoretical K_{α} resonance strengths for successively higher ionization states of Al (upper panel). The experimental data in the lower panel exhibit overlaps and different total intensities of the various K_{α} complexes. That is also seen qualitatively in the top panel with aggregate K_{α} resonance strengths for each ion. In the calculations presented, and comparison with the LCLS-XFEL experiment, we have considered only thermal broadening, and neglected intrinsic broadening effects such as Auger widths. That is because external broadening due to transient warm dense matter conditions in the experiment pertain to rapidly varying temperatures and densities, and likely to be much greater than autoionization widths. However, a more detailed model should include both intrinsic inner-shell and extrinsic plasma effects, as well as broadening, smearing, and dissolution of resonances as a function of temperature and density.

Ti has been the other proposed element of possible interest for observation of fluorescence at LCLS-XFEL. Cu is also readily available for observation of the effect. Fig. 4 shows the K_{α} resonance complexes for titanium and copper. Structures similar to Al are evident. While for Al ions K_{α} resonance fluorescence occurs in the 1.48–1.88 keV range, the corresponding range for Ti K_{α} resonances is 4.5–5 keV and 8.0–8.7 keV for copper (Table 2). The possibility of experimental observations of Ti K_{α} resonances at the LCLS-XFEL suggests itself since the averaged energies and

Table 1

Parameters for resonant K_{α} (1s–2p) transitions of various ionization stages, from H- to F-like ions, of Al. Auger cascades are initiated with K-shell ionization leading to these various ionization stages. N_t is number of E1 transitions.

Transition array	Ion state	$N_t E(K_{\alpha})$	$E(K_{\alpha})$ (keV)	$\langle f_{tot} \rangle$	$\langle \sigma_{res} \rangle$ (Mb)	$\langle \kappa \rangle$ (cm^2/g)
1s–2p	H	2	1.7289	0.413	3.33	7.43E+04
1s ² –1s2p	He	2	1.5992	0.758	6.11	1.36E+05
1s ² 2s–1s2s2p	Li	6	1.5865	0.706	5.70	1.27E+05
1s ² 2s ² –1s2s ² 2p	Be	2	1.5738	0.611	4.93	1.10E+05
1s ² 2s ² 2p–1s2s ² 2p ²	B	14	1.5556	1.017	8.20	1.83E+05
1s ² 2s ² 2p ² –1s2s ² 2p ³	C	35	1.5394	1.907	15.4	3.43E+05
1s ² 2s ² 2p ³ –1s2s ² 2p ⁴	N	35	1.5218	1.385	11.2	2.49E+05
1s ² 2s ² 2p ⁴ –1s2s ² 2p ⁵	O	14	1.5087	0.875	7.05	1.57E+05
1s ² 2s ² 2p ⁵ –1s2s ² 2p ⁶	F	2	1.4913	0.173	1.40	3.12E+04

Table 2

Transition parameters, f_{ij} , S , A_{ji} , and resonant cross section σ_{pl} for 1s–2p K_α transitions in Al, Ti, and Cu ions. The configuration numbers C_{ij} correspond to configurations specified in the top row of the sets.

Z	N_e	$SL\pi C_i$	$SL\pi C_j$	g_i	g_j	$\lambda (\text{\AA})$	E (keV)	$E_i (\text{Ry})$	$E_j (\text{Ry})$	f_{ij}	S	$A_{ji} (\text{s}^{-1})$	$\sigma_{pl} (\text{Mb})$
Al¹²⁺: $C_i(1)=1s$, $C_j(3)=2p$, $E_K \geq -2.16 \text{ keV}$													
13	1	2Se 1	2Po 3	2	2	7.170	1.729	0.00	127.01	1.38E–01	6.50E–03	1.78E+13	1.11E+00
13	1	2Se 1	2Po 3	2	4	7.170	1.729	0.00	127.11	2.75E–01	1.30E–02	1.78E+13	2.22E+00
Total: no. of trans=2							E (keV)=1.729	$\langle f \rangle$, $\langle \sigma_{\text{res}} \rangle$, $\langle \kappa \rangle =$		4.13E–01	3.33E+00	7.43E+04	
Al¹¹⁺: $C_i(1)=1s1s$, $C_j(3)=1s2p$													
13	2	1Se 1	1Po 3	1	3	7.753	1.599	0.00	117.54	7.56E–01	1.93E–02	2.80E+13	6.10E+00
13	2	1Se 1	3Po 3	1	3	7.80	1.589	0.00	116.76	1.72E–03	4.41E–05	6.26E+10	1.38E–02
Total: no. of trans=2							E (keV)=1.599	$\langle f \rangle$, $\langle \sigma_{\text{res}} \rangle$, $\langle \kappa \rangle =$		7.58E–01	6.11E+00	1.36E+05	
Al¹⁰⁺: $C_i(1)=1s1s2s$, $C_j(11)=1s2s2p$													
13	3	2Se 1	2Po11	2	2	7.838	1.582	0.00	116.26	2.07E–01	1.07E–02	2.25E+13	1.67E+00
13	3	2Se 1	2Po11	2	4	7.836	1.582	0.00	116.29	4.34E–01	2.24E–02	2.36E+13	3.50E+00
13	3	2Se 1	2Po11	2	2	7.795	1.591	0.00	116.91	2.82E–02	1.45E–03	3.10E+12	2.28E–01
13	3	2Se 1	2Po11	2	4	7.793	1.591	0.00	116.93	3.68E–02	1.89E–03	2.02E+12	2.97E–01
13	3	2Se 1	4Po11	2	2	7.92	1.565	0.00	115.01	4.20E–05	2.19E–06	4.46E+09	3.39E–04
13	3	2Se 1	4Po11	2	4	7.92	1.565	0.00	115.03	2.21E–04	1.15E–05	1.17E+10	1.78E–03
Total: no. of trans=6							E (keV)=1.586	$\langle f \rangle$, $\langle \sigma_{\text{res}} \rangle$, $\langle \kappa \rangle =$		7.06E–01	5.70E+00	1.27E+05	
Al¹⁹⁺: $C_i(1)=1s1s2s2s$, $C_j(28)=1s2s2s2p$													
13	4	1Se 1	1Po28	1	3	7.878	1.574	0.00	115.67	6.10E–01	1.58E–02	2.19E+13	4.92E+00
13	4	1Se 1	3Po28	1	3	7.92	1.565	0.00	115.06	1.24E–03	3.22E–05	4.38E+10	9.97E–03
Total: no. of trans=2							E (keV)=1.574	$\langle f \rangle$, $\langle \sigma_{\text{res}} \rangle$, $\langle \kappa \rangle =$		6.11E–01	4.93E+00	1.10E+05	
Al⁸⁺: $C_i(1)=1s1s2s2s2p$, $C_j(23)=1s2s2s2p2p$													
13	5	2Po 1	2De23	2	4	7.978	1.554	0.00	114.23	2.07E–01	1.09E–02	1.08E+13	1.67E+00
13	5	2Po 1	2De23	4	4	7.981	1.553	0.05	114.23	2.12E–03	2.23E–04	2.22E+11	1.71E–02
13	5	2Po 1	2De23	4	6	7.981	1.553	0.05	114.23	1.50E–01	1.58E–02	1.05E+13	1.21E+00
13	5	2Po 1	2Pe23	2	2	7.970	1.556	0.00	114.34	2.15E–01	1.13E–02	2.26E+13	1.73E+00
13	5	2Po 1	2Pe23	4	2	7.974	1.555	0.05	114.34	4.71E–02	4.95E–03	9.88E+12	3.80E–01
13	5	2Po 1	2Pe23	2	4	7.967	1.556	0.00	114.38	6.33E–02	3.32E–03	3.33E+12	5.10E–01
13	5	2Po 1	2Pe23	4	4	7.971	1.555	0.05	114.38	2.72E–01	2.86E–02	2.86E+13	2.20E+00
13	5	2Po 1	2Se23	2	2	7.931	1.563	0.00	114.90	2.36E–02	1.23E–03	2.50E+12	1.90E–01
13	5	2Po 1	2Se23	4	2	7.935	1.562	0.05	114.90	3.64E–02	3.80E–03	7.71E+12	2.93E–01
13	5	2Po 1	4Pe23	2	2	8.03	1.544	0.00	113.46	1.14E–04	6.02E–06	1.18E+10	9.19E–04
13	5	2Po 1	4Pe23	4	2	8.04	1.543	0.05	113.46	8.80E–06	9.32E–07	1.82E+09	7.10E–05
13	5	2Po 1	4Pe23	2	4	8.03	1.544	0.00	113.48	7.41E–07	3.92E–08	3.83E+07	5.98E–06
13	5	2Po 1	4Pe23	4	4	8.03	1.543	0.05	113.48	9.39E–05	9.93E–06	9.70E+09	7.57E–04
13	5	2Po 1	4Pe23	4	6	8.03	1.544	0.05	113.51	2.14E–04	2.26E–05	1.47E+10	1.72E–03
Total: no. of trans=14							E (keV)=1.556	$\langle f \rangle$, $\langle \sigma_{\text{res}} \rangle$, $\langle \kappa \rangle =$		1.02E+00	8.20E+00	1.83E+05	
Al⁷⁺: $C_i(1)=1s1s2s2s2p2p$, $C_j(17)=1s2s2s2p2p2p$													
13	6	3Pe 1	3Do17	1	3	8.065	1.537	0.00	112.99	1.73E–01	4.60E–03	5.92E+12	1.40E+00
13	6	3Pe 1	3Do17	3	3	8.066	1.537	0.02	112.99	3.42E–02	2.72E–03	3.50E+12	2.76E–01
13	6	3Pe 1	3Do17	5	3	8.069	1.537	0.05	112.99	1.32E–03	1.75E–04	2.25E+11	1.06E–02
13	6	3Pe 1	3Do17	3	5	8.066	1.537	0.02	112.99	1.27E–01	1.01E–02	7.79E+12	1.02E+00
13	6	3Pe 1	3Do17	5	5	8.069	1.537	0.05	112.99	1.79E–02	2.38E–03	1.83E+12	1.44E–01
13	6	3Pe 1	3Do17	5	7	8.069	1.537	0.05	112.99	1.31E–01	1.74E–02	9.59E+12	1.06E+00
13	6	3Pe 1	3So17	1	3	8.054	1.539	0.00	113.15	1.43E–01	3.79E–03	4.90E+12	1.15E+00
13	6	3Pe 1	3So17	3	3	8.055	1.539	0.02	113.15	1.41E–01	1.13E–02	1.45E+13	1.14E+00
13	6	3Pe 1	3So17	5	3	8.057	1.539	0.05	113.15	1.22E–01	1.61E–02	2.08E+13	9.81E–01
13	6	3Pe 1	3Po17	3	5	8.037	1.543	0.02	113.40	2.81E–02	2.23E–03	1.74E+12	2.27E–01
13	6	3Pe 1	3Po17	5	5	8.040	1.542	0.05	113.40	7.53E–02	9.96E–03	7.77E+12	6.07E–01
13	6	3Pe 1	3Po17	3	1	8.037	1.543	0.02	113.40	3.10E–02	2.46E–03	9.61E+12	2.50E–01

Table 2 (continued)

Z	N_e	$SL\pi C_i$	$SL\pi C_j$	g_i	g_j	$\lambda (\text{\AA})$	E (keV)	E_i (Ry)	E_j (Ry)	f_{ij}	S	$A_{ji} (\text{s}^{-1})$	$\sigma_{Pl} (\text{Mb})$
13	6	3Pe 1	3Po17	1	3	8.035	1.543	0.00	113.41	6.49E-02	1.72E-03	2.24E+12	5.23E-01
13	6	3Pe 1	3Po17	3	3	8.037	1.543	0.02	113.41	1.81E-02	1.44E-03	1.87E+12	1.46E-01
13	6	3Pe 1	3Po17	5	3	8.039	1.542	0.05	113.41	3.29E-02	4.36E-03	5.66E+12	2.66E-01
13	6	1De 1	1Do17	5	5	8.060	1.538	0.46	113.51	2.80E-01	3.72E-02	2.88E+13	2.26E+00
13	6	1De 1	1Po17	5	3	8.031	1.544	0.46	113.92	9.70E-02	1.28E-02	1.67E+13	7.82E-01
13	6	1Se 1	1Po17	1	3	8.062	1.538	0.89	113.92	3.75E-01	9.96E-03	1.28E+13	3.02E+00
13	6	3Pe 1	5So17	3	5	8.13	1.525	0.02	112.12	3.00E-05	2.41E-06	1.82E+09	2.42E-04
13	6	3Pe 1	5So17	5	5	8.13	1.525	0.05	112.12	4.64E-05	6.21E-06	4.68E+09	3.74E-04
13	6	1De 1	5So17	5	5	8.16	1.519	0.46	112.12	2.34E-08	3.14E-09	2.34E+06	1.89E-07
13	6	1De 1	3Do17	5	3	8.10	1.531	0.46	112.99	6.92E-05	9.22E-06	1.17E+10	5.58E-04
13	6	1Se 1	3Do17	1	3	8.13	1.525	0.89	112.99	4.82E-06	1.29E-07	1.62E+08	3.89E-05
13	6	1De 1	3Do17	5	5	8.10	1.531	0.46	112.99	9.20E-05	1.23E-05	9.36E+09	7.42E-04
13	6	1De 1	3Do17	5	7	8.10	1.531	0.46	112.99	4.47E-04	5.96E-05	3.25E+10	3.61E-03
13	6	1De 1	3So17	5	3	8.09	1.533	0.46	113.15	8.89E-05	1.18E-05	1.51E+10	7.17E-04
13	6	1Se 1	3So17	1	3	8.12	1.527	0.89	113.15	7.42E-07	1.98E-08	2.50E+07	5.98E-06
13	6	1De 1	3Po17	5	5	8.07	1.537	0.46	113.40	1.00E-02	1.33E-03	1.03E+12	8.08E-02
13	6	1De 1	3Po17	5	3	8.07	1.537	0.46	113.41	6.97E-05	9.25E-06	1.19E+10	5.62E-04
13	6	1Se 1	3Po17	1	3	8.10	1.531	0.89	113.41	3.37E-04	8.98E-06	1.14E+10	2.71E-03
13	6	3Pe 1	1Do17	3	5	8.03	1.544	0.02	113.51	1.45E-03	1.15E-04	9.02E+10	1.17E-02
13	6	3Pe 1	1Do17	5	5	8.03	1.544	0.05	113.51	7.55E-04	9.98E-05	7.81E+10	6.09E-03
13	6	3Pe 1	1Po17	1	3	8.00	1.550	0.00	113.92	6.63E-05	1.75E-06	2.30E+09	5.35E-04
13	6	3Pe 1	1Po17	3	3	8.00	1.550	0.02	113.92	3.68E-05	2.91E-06	3.83E+09	2.97E-04
13	6	3Pe 1	1Po17	5	3	8.00	1.549	0.05	113.92	1.19E-05	1.57E-06	2.07E+09	9.60E-05
Total: no. of trans=35		$E (\text{keV}) = 1.539$		$\langle f \rangle, \langle \sigma_{\text{res}} \rangle, \langle \kappa \rangle =$		1.91E+00		1.54E+01		3.43E+05			
Al ⁶⁺ : $C_i(1)=1s1s2s2s2p2p2p$, $C_j(14)=1s2s2s2p2p2p2p$													
13	7	4So 1	4Pe14	4	6	8.147	1.522	0.00	111.85	1.35E-01	1.45E-02	9.04E+12	1.09E+00
13	7	4So 1	4Pe14	4	4	8.146	1.522	0.00	111.87	9.01E-02	9.66E-03	9.05E+12	7.26E-01
13	7	4So 1	4Pe14	4	2	8.144	1.522	0.00	111.89	4.51E-02	4.83E-03	9.06E+12	3.63E-01
13	7	2Do 1	2De14	4	4	8.144	1.522	0.60	112.50	1.57E-01	1.68E-02	1.58E+13	1.26E+00
13	7	2Do 1	2De14	6	4	8.144	1.522	0.61	112.50	7.79E-05	1.25E-05	1.18E+10	6.28E-04
13	7	2Po 1	2De14	2	4	8.163	1.519	0.87	112.50	4.82E-02	2.59E-03	2.41E+12	3.89E-01
13	7	2Po 1	2De14	4	4	8.164	1.519	0.88	112.50	1.22E-02	1.31E-03	1.22E+12	9.81E-02
13	7	2Do 1	2De14	4	6	8.143	1.523	0.60	112.51	6.75E-03	7.24E-04	4.53E+11	5.45E-02
3	7	2Do 1	2De14	6	6	8.144	1.522	0.61	112.51	1.29E-01	2.07E-02	1.29E+13	1.04E+00
13	7	2Po 1	2De14	4	6	8.163	1.519	0.88	112.51	7.51E-02	8.07E-03	5.01E+12	6.05E-01
13	7	2Do 1	2Pe14	4	4	8.137	1.524	0.60	112.60	1.27E-02	1.36E-03	1.28E+12	1.02E-01
13	7	2Do 1	2Pe14	6	4	8.137	1.524	0.61	112.60	1.53E-01	2.46E-02	2.31E+13	1.23E+00
13	7	2Po 1	2Pe14	2	4	8.157	1.520	0.87	112.60	7.41E-02	3.98E-03	3.72E+12	5.98E-01
13	7	2Po 1	2Pe14	4	4	8.157	1.520	0.88	112.60	9.09E-02	9.77E-03	9.12E+12	7.33E-01
13	7	2Do 1	2Pe14	4	2	8.135	1.524	0.60	112.62	1.05E-01	1.13E-02	2.12E+13	8.49E-01
13	7	2Po 1	2Pe14	2	2	8.155	1.520	0.87	112.62	1.02E-01	5.46E-03	1.02E+13	8.20E-01
13	7	2Po 1	2Pe14	4	2	8.155	1.520	0.88	112.62	3.36E-02	3.60E-03	6.73E+12	2.71E-01
13	7	2Po 1	2Se14	2	2	8.119	1.527	0.87	113.11	5.17E-02	2.76E-03	5.23E+12	4.17E-01
13	7	2Po 1	2Se14	4	2	8.120	1.527	0.88	113.11	6.40E-02	6.84E-03	1.29E+13	5.16E-01
13	7	2Do 1	4Pe14	4	6	8.19	1.513	0.60	111.85	2.88E-05	3.11E-06	1.91E+09	2.33E-04
13	7	2Do 1	4Pe14	6	6	8.19	1.513	0.61	111.85	1.52E-04	2.46E-05	1.51E+10	1.22E-03
13	7	2Po 1	4Pe14	4	6	8.21	1.510	0.88	111.85	1.45E-05	1.57E-06	9.55E+08	1.17E-04
13	7	2Do 1	4Pe14	4	4	8.19	1.514	0.60	111.87	4.60E-05	4.97E-06	4.58E+09	3.71E-04
13	7	2Do 1	4Pe14	6	4	8.19	1.514	0.61	111.87	2.52E-05	4.07E-06	3.75E+09	2.03E-04
13	7	2Po 1	4Pe14	2	4	8.21	1.510	0.87	111.87	2.32E-07	1.26E-08	1.15E+07	1.87E-06

13	7	2Po 1	4Pe14	4	4	8.21	1.510	0.88	111.87	2.25E-05	2.43E-06	2.22E+09	1.81E-04	
13	7	2Do 1	4Pe14	4	2	8.19	1.514	0.60	111.89	1.21E-05	1.30E-06	2.40E+09	9.72E-05	
13	7	2Po 1	4Pe14	2	2	8.21	1.510	0.87	111.89	2.09E-05	1.13E-06	2.07E+09	1.69E-04	
13	7	2Po 1	4Pe14	4	2	8.21	1.510	0.88	111.89	2.25E-06	2.43E-07	4.45E+08	1.81E-05	
13	7	4So 1	2De14	4	4	8.10	1.531	0.00	112.50	1.33E-06	1.41E-07	1.35E+08	1.07E-05	
13	7	4So 1	2De14	4	6	8.10	1.531	0.00	112.51	1.10E-05	1.17E-06	7.43E+08	8.84E-05	
13	7	4So 1	2Pe14	4	4	8.09	1.532	0.00	112.60	5.99E-05	6.39E-06	6.10E+09	4.83E-04	
13	7	4So 1	2Pe14	4	2	8.09	1.532	0.00	112.62	7.77E-06	8.28E-07	1.58E+09	6.27E-05	
13	7	4So 1	2Se14	4	2	8.06	1.539	0.00	113.11	7.36E-06	7.81E-07	1.51E+09	5.93E-05	
13	7	2Do 1	2Se14	4	2	8.10	1.531	0.60	113.11	2.05E-04	2.18E-05	4.16E+10	1.65E-03	
Total: no. of trans=35				E (keV)=1.522				<f>, < σ_{res} >, < κ > =				1.39E+00	1.12E+01	2.49E+05
Al ⁵⁺ : C _i (1)=1s1s2s2s2p2p2p2p, C _j (18)=1s2s2s2p2p2p2p2p														
13	8	3Pe 1	3Po18	5	5	8.218	1.509	0.00	110.89	1.29E-01	1.75E-02	1.28E+13	1.04E+00	
13	8	3Pe 1	3Po18	3	5	8.220	1.508	0.03	110.89	7.20E-02	5.85E-03	4.27E+12	5.81E-01	
13	8	3Pe 1	3Po18	5	3	8.216	1.509	0.00	110.91	4.35E-02	5.88E-03	7.16E+12	3.51E-01	
13	8	3Pe 1	3Po18	3	3	8.218	1.509	0.03	110.91	4.31E-02	3.50E-03	4.26E+12	3.48E-01	
13	8	3Pe 1	3Po18	1	3	8.219	1.509	0.04	110.91	1.73E-01	4.68E-03	5.69E+12	1.39E+00	
13	8	3Pe 1	3Po18	3	1	8.217	1.509	0.03	110.93	5.76E-02	4.68E-03	1.71E+13	4.65E-01	
13	8	1De 1	1Po18	5	3	8.213	1.510	0.40	111.36	1.80E-01	2.43E-02	2.97E+13	1.45E+00	
13	8	1Se 1	1Po18	1	3	8.242	1.504	0.80	111.36	1.76E-01	4.76E-03	5.74E+12	1.42E+00	
13	8	1De 1	3Po18	5	5	8.25	1.503	0.40	110.89	3.53E-04	4.80E-05	3.46E+10	2.85E-03	
13	8	1De 1	3Po18	5	3	8.25	1.504	0.40	110.91	8.46E-05	1.15E-05	1.38E+10	6.82E-04	
13	8	1Se 1	3Po18	1	3	8.28	1.498	0.80	110.91	9.08E-06	2.47E-07	2.95E+08	7.32E-05	
13	8	3Pe 1	1Po18	5	3	8.18	1.515	0.00	111.36	1.53E-04	2.06E-05	2.54E+10	1.23E-03	
13	8	3Pe 1	1Po18	3	3	8.19	1.515	0.03	111.36	9.71E-05	7.85E-06	9.67E+09	7.83E-04	
13	8	3Pe 1	1Po18	1	3	8.19	1.515	0.04	111.36	1.23E-05	3.31E-07	4.07E+08	9.89E-05	
Total: no. of trans=14				E (keV)=1.509				<f>, < σ_{res} >, < κ > =				8.75E-01	7.05E+00	1.57E+05
Al ⁴⁺ : C _i (1)=1s1s2s2s2p2p2p2p2p, C _j (16)=1s2s2s2p2p2p2p2p														
13	9	2Po 1	2Se16	4	2	8.313	1.491	0.00	109.62	8.67E-02	9.49E-03	1.67E+13	6.99E-01	
13	9	2Po 1	2Se16	2	2	8.316	1.491	0.04	109.62	8.66E-02	4.74E-03	8.35E+12	6.98E-01	
Total: no. of trans=2				E (keV)=1.491				<f>, < σ_{res} >, < κ > =				1.73E-01	1.40E+00	3.12E+04
Ti ²¹⁺ : C _i (1)=1s, C _j (3)=2p, E _K ≥ 6.21 keV														
22	1	2Se 1	2Po 3	2	2	2.496	4.967	0.00	365.15	1.36E-01	2.23E-03	1.45E+14	1.09E+00	
22	1	2Se 1	2Po 3	2	4	2.490	4.979	0.00	365.94	2.71E-01	4.44E-03	1.46E+14	2.18E+00	
Total: no. of trans=2				E (keV)=4.975				<f>, < σ_{res} >, < κ > =				4.06E-01	3.28E+00	4.12E+04
Ti ²⁰⁺ : C _i (1)=1s1s, C _j (3)=1s2p														
22	2	1Se 1	1Po 3	1	3	2.607	4.756	0.00	349.49	7.44E-01	6.39E-03	2.43E+14	6.00E+00	
22	2	1Se 1	3Po 3	1	3	2.62	4.732	0.00	347.77	2.96E-02	2.56E-04	9.60E+12	2.39E-01	
Total: no. of trans=2				E (keV)=4.755				<f>, < σ_{res} >, < κ > =				7.74E-01	6.24E+00	7.85E+04
Ti ¹⁹⁺ : C _i (1)=1s1s2s, C _j (11)=1s2s2p														
22	3	2Se 1	2Po11	2	2	2.626	4.721	0.00	347.01	1.79E-01	3.10E-03	1.74E+14	1.45E+00	
22	3	2Se 1	2Po11	2	4	2.624	4.725	0.00	347.34	4.76E-01	8.22E-03	2.31E+14	3.84E+00	
22	3	2Se 1	2Po11	2	2	2.617	4.738	0.00	348.24	6.80E-02	1.17E-03	6.63E+13	5.49E-01	
22	3	2Se 1	2Po11	2	4	2.616	4.739	0.00	348.37	1.53E-02	2.63E-04	7.45E+12	1.23E-01	
22	3	2Se 1	4Po11	2	2	2.65	4.687	0.00	344.58	8.98E-04	1.56E-05	8.56E+11	7.24E-03	
22	3	2Se 1	4Po11	2	4	2.64	4.691	0.00	344.77	5.60E-03	9.75E-05	2.67E+12	4.52E-02	
Total: no. of trans=6				E (keV)=4.732				<f>, < σ_{res} >, < κ > =				7.45E-01	6.01E+00	7.56E+04
Ti ¹⁸⁺ : C _i (1)=1s1s2s2s, C _j (28)=1s2s2p2p														
22	4	1Se 1	1Po28	1	3	2.634	4.707	0.00	346.00	6.53E-01	5.66E-03	2.09E+14	5.27E+00	
22	4	1Se 1	3Po28	1	3	2.65	4.687	0.00	344.50	2.44E-02	2.13E-04	7.77E+12	1.97E-01	
Total: no. of trans=2				E (keV)=4.708				<f>, < σ_{res} >, < κ > =				6.78E-01	5.47E+00	6.88E+04
Ti ¹⁷⁺ : C _i (1)=1s1s2s2s2p, C _j (23)=1s2s2s2p2p														
22	5	2Po 1	2De23	2	4	2.654	4.672	0.00	343.30	2.85E-01	4.99E-03	1.35E+14	2.30E+00	
22	5	2Po 1	2De23	4	4	2.659	4.663	0.57	343.30	7.58E-03	2.65E-04	7.15E+12	6.11E-02	

Table 2 (continued)

Z	N_e	$SL\pi C_i$	$SL\pi C_j$	g_i	g_j	λ (Å)	E (keV)	E_i (Ry)	E_j (Ry)	f_{ij}	S	A_{ji} (s^{-1})	σ_{pl} (Mb)
22	5	2Po 1	2Pe23	2	2	2.653	4.673	0.00	343.44	2.58E-01	4.51E-03	2.44E+14	2.08E+00
22	5	2Po 1	2Pe23	4	2	2.658	4.665	0.57	343.44	3.67E-02	1.28E-03	6.92E+13	2.96E-01
22	5	2Po 1	2De23	4	6	2.658	4.665	0.57	343.46	1.63E-01	5.70E-03	1.02E+14	1.31E+00
22	5	2Po 1	2Pe23	2	4	2.649	4.680	0.00	344.02	1.96E-02	3.41E-04	9.30E+12	1.58E-01
22	5	2Po 1	2Pe23	4	4	2.653	4.673	0.57	344.02	2.97E-01	1.04E-02	2.82E+14	2.40E+00
22	5	2Po 1	2Se23	2	2	2.643	4.691	0.00	344.78	5.36E-03	9.32E-05	5.11E+12	4.32E-02
22	5	2Po 1	2Se23	4	2	2.647	4.684	0.57	344.78	5.71E-02	1.99E-03	1.09E+14	4.61E-01
22	5	2Po 1	4Pe23	2	2	2.67	4.647	0.00	341.57	4.14E-03	7.27E-05	3.88E+12	3.34E-02
22	5	2Po 1	4Pe23	4	2	2.67	4.640	0.57	341.57	1.38E-04	4.85E-06	2.58E+11	1.11E-03
22	5	2Po 1	4Pe23	2	4	2.67	4.651	0.00	341.83	3.06E-05	5.37E-07	1.44E+10	2.47E-04
22	5	2Po 1	4Pe23	4	4	2.67	4.644	0.57	341.83	1.80E-03	6.34E-05	1.69E+12	1.45E-02
22	5	2Po 1	4Pe23	4	6	2.67	4.647	0.57	342.11	7.63E-03	2.68E-04	4.76E+12	6.15E-02
Total: no. of trans=14				E (keV)=4.671			$\langle f \rangle, \langle \sigma_{res} \rangle, \langle \kappa \rangle =$			1.14E+00	9.22E+00	1.16E+05	
Ti ¹⁶⁺ : C _i (1)=1s1s2s2s2p2p, C _j (17)=1s2s2s2p2p2p													
22	6	3Pe 1	3Do17	1	3	2.673	4.638	0.00	340.90	3.27E-01	2.88E-03	1.02E+14	2.64E+00
22	6	3Pe 1	3Do17	3	3	2.676	4.633	0.31	340.90	6.78E-03	1.79E-04	6.32E+12	5.47E-02
22	6	3Pe 1	3Do17	5	3	2.678	4.630	0.58	340.90	6.52E-03	2.87E-04	1.01E+13	5.26E-02
22	6	3Pe 1	3Do17	3	5	2.675	4.635	0.31	340.93	1.75E-01	4.63E-03	9.79E+13	1.41E+00
22	6	3Pe 1	3Do17	5	5	2.678	4.630	0.58	340.93	2.21E-03	9.74E-05	2.06E+12	1.78E-02
22	6	3Pe 1	3Do17	5	7	2.677	4.631	0.58	341.03	1.37E-01	6.02E-03	9.09E+13	1.10E+00
22	6	3Pe 1	3So17	1	3	2.669	4.645	0.00	341.41	1.11E-01	9.80E-04	3.48E+13	8.99E-01
22	6	3Pe 1	3So17	3	3	2.672	4.640	0.31	341.41	2.13E-01	5.62E-03	1.99E+14	1.72E+00
22	6	3Pe 1	3So17	5	3	2.674	4.637	0.58	341.41	8.13E-02	3.58E-03	1.26E+14	6.55E-01
22	6	3Pe 1	3Po17	3	5	2.668	4.647	0.31	341.81	2.08E-03	5.47E-05	1.17E+12	1.67E-02
22	6	3Pe 1	3Po17	5	5	2.671	4.642	0.58	341.81	1.32E-01	5.80E-03	1.23E+14	1.06E+00
22	6	3Pe 1	3Po17	3	1	2.668	4.647	0.31	341.83	3.64E-02	9.58E-04	1.02E+14	2.93E-01
22	6	3Pe 1	3Po17	1	3	2.665	4.652	0.00	341.95	4.54E-03	3.98E-05	1.42E+12	3.66E-02
22	6	3Pe 1	3Po17	3	3	2.667	4.649	0.31	341.95	3.41E-03	8.99E-05	3.20E+12	2.75E-02
22	6	3Pe 1	3Po17	5	3	2.669	4.645	0.58	341.95	8.36E-02	3.67E-03	1.30E+14	6.74E-01
22	6	1De 1	1Do17	5	5	2.673	4.638	1.39	342.33	2.56E-01	1.13E-02	2.39E+14	2.07E+00
22	6	1De 1	1Po17	5	3	2.667	4.649	1.39	343.06	1.12E-01	4.91E-03	1.75E+14	9.01E-01
22	6	1Se 1	1Po17	1	3	2.674	4.637	2.30	343.06	4.22E-01	3.71E-03	1.31E+14	3.40E+00
22	6	3Pe 1	5So17	3	5	2.69	4.611	0.31	339.24	1.62E-03	4.29E-05	8.95E+11	1.30E-02
22	6	3Pe 1	5So17	5	5	2.69	4.607	0.58	339.24	1.39E-03	6.15E-05	1.28E+12	1.12E-02
22	6	1De 1	5So17	5	5	2.70	4.597	1.39	339.24	3.01E-05	1.34E-06	2.76E+10	2.43E-04
22	6	1De 1	3Do17	5	3	2.68	4.619	1.39	340.90	1.16E-03	5.14E-05	1.79E+12	9.38E-03
22	6	1Se 1	3Do17	1	3	2.69	4.607	2.30	340.90	2.73E-04	2.42E-06	8.37E+10	2.20E-03
22	6	1De 1	3Do17	5	5	2.68	4.619	1.39	340.93	3.49E-03	1.54E-04	3.23E+12	2.81E-02
22	6	1De 1	3Do17	5	7	2.68	4.621	1.39	341.03	1.77E-02	7.81E-04	1.17E+13	1.43E-01
22	6	1De 1	3So17	5	3	2.68	4.626	1.39	341.41	3.88E-03	1.71E-04	6.00E+12	3.13E-02
22	6	1Se 1	3So17	1	3	2.69	4.614	2.30	341.41	9.43E-06	8.34E-08	2.90E+09	7.60E-05
22	6	1De 1	3Po17	5	5	2.68	4.631	1.39	341.81	5.05E-02	2.22E-03	4.70E+13	4.07E-01
22	6	1De 1	3Po17	5	3	2.68	4.633	1.39	341.95	2.20E-03	9.70E-05	3.42E+12	1.78E-02
22	6	1Se 1	3Po17	1	3	2.68	4.621	2.30	341.95	1.58E-02	1.40E-04	4.89E+12	1.28E-01
22	6	3Pe 1	1Do17	3	5	2.66	4.654	0.31	342.33	4.65E-03	1.22E-04	2.62E+12	3.75E-02
22	6	3Pe 1	1Do17	5	5	2.67	4.649	0.58	342.33	1.35E-04	5.91E-06	1.26E+11	1.08E-03
22	6	3Pe 1	1Po17	1	3	2.66	4.668	0.00	343.06	7.35E-04	6.43E-06	2.32E+11	5.93E-03
22	6	3Pe 1	1Po17	3	3	2.66	4.663	0.31	343.06	8.76E-04	2.30E-05	8.26E+11	7.06E-03
22	6	3Pe 1	1Po17	5	3	2.66	4.659	0.58	343.06	4.20E-04	1.84E-05	6.59E+11	3.39E-03
Total: no. of trans=35				E (keV)=4.639			$\langle f \rangle, \langle \sigma_{res} \rangle, \langle \kappa \rangle =$			2.22E+00	1.79E+01	2.25E+05	

Ti ¹⁵⁺ : C _i (1)=1s1s2s2s2p2p2p, C _j (14)=1s2s2s2p2p2p2p	22	7	4So 1	4Pe14	4	6	2.694	4.602	0.00	338.21	1.57E–01	5.58E–03	9.64E+13	1.27E+00
	22	7	4So 1	4Pe14	4	4	2.692	4.606	0.00	338.52	1.10E–01	3.91E–03	1.02E+14	8.89E–01
	22	7	4So 1	4Pe14	4	2	2.691	4.607	0.00	338.65	5.46E–02	1.94E–03	1.01E+14	4.40E–01
	22	7	2Do 1	2De14	4	4	2.692	4.606	1.08	339.62	2.40E–01	8.50E–03	2.21E+14	1.93E+00
	22	7	2Do 1	2De14	6	4	2.693	4.604	1.26	339.62	1.77E–02	9.41E–04	2.44E+13	1.43E–01
	22	7	2Po 1	2De14	2	4	2.698	4.595	1.84	339.62	1.53E–02	2.72E–04	7.03E+12	1.24E–01
	22	7	2Po 1	2De14	4	4	2.700	4.592	2.09	339.62	6.47E–03	2.30E–04	5.92E+12	5.22E–02
	22	7	2Do 1	2De14	4	6	2.690	4.609	1.08	339.79	1.14E–04	4.02E–06	6.98E+10	9.16E–04
	22	7	2Do 1	2De14	6	6	2.692	4.606	1.26	339.79	1.49E–01	7.94E–03	1.38E+14	1.20E+00
	22	7	2Po 1	2De14	4	6	2.698	4.595	2.09	339.79	9.93E–02	3.53E–03	6.06E+13	8.00E–01
	22	7	2Do 1	2Pe14	4	4	2.688	4.613	1.08	340.09	1.89E–03	6.68E–05	1.74E+12	1.52E–02
	22	7	2Do 1	2Pe14	6	4	2.689	4.611	1.26	340.09	1.60E–01	8.48E–03	2.21E+14	1.29E+00
	22	7	2Po 1	2Pe14	2	4	2.694	4.602	1.84	340.09	1.31E–01	2.32E–03	6.01E+13	1.05E+00
	22	7	2Po 1	2Pe14	4	4	2.696	4.599	2.09	340.09	6.86E–02	2.44E–03	6.30E+13	5.53E–01
	22	7	2Do 1	2Pe14	4	2	2.687	4.614	1.08	340.18	8.48E–02	3.00E–03	1.57E+14	6.84E–01
	22	7	2Po 1	2Pe14	2	2	2.693	4.604	1.84	340.18	1.63E–01	2.89E–03	1.50E+14	1.32E+00
	22	7	2Po 1	2Pe14	4	2	2.695	4.601	2.09	340.18	4.18E–02	1.48E–03	7.68E+13	3.37E–01
	22	7	2Po 1	2Se14	2	2	2.686	4.616	1.84	341.10	1.70E–02	3.00E–04	1.57E+13	1.37E–01
	22	7	2Po 1	2Se14	4	2	2.688	4.613	2.09	341.10	1.10E–01	3.91E–03	2.04E+14	8.91E–01
	22	7	2Do 1	4Pe14	4	6	2.70	4.587	1.08	338.21	3.31E–03	1.18E–04	2.01E+12	2.67E–02
	22	7	2Do 1	4Pe14	6	6	2.70	4.585	1.26	338.21	3.98E–03	2.13E–04	3.63E+12	3.21E–02
	22	7	2Po 1	4Pe14	4	6	2.71	4.573	2.09	338.21	1.64E–04	5.85E–06	9.92E+10	1.32E–03
	22	7	2Do 1	4Pe14	4	4	2.70	4.590	1.08	338.52	6.56E–04	2.33E–05	6.00E+11	5.29E–03
	22	7	2Do 1	4Pe14	6	4	2.70	4.589	1.26	338.52	1.15E–03	6.14E–05	1.58E+12	9.27E–03
	22	7	2Po 1	4Pe14	2	4	2.71	4.580	1.84	338.52	2.91E–05	5.19E–07	1.33E+10	2.35E–04
	22	7	2Po 1	4Pe14	4	4	2.71	4.577	2.09	338.52	9.69E–04	3.46E–05	8.81E+11	7.82E–03
	22	7	2Do 1	4Pe14	4	2	2.70	4.594	1.08	338.65	3.69E–04	1.31E–05	6.76E+11	2.98E–03
	22	7	2Po 1	4Pe14	2	2	2.71	4.582	1.84	338.65	1.64E–03	2.93E–05	1.50E+12	1.33E–02
	22	7	2Po 1	4Pe14	4	2	2.71	4.578	2.09	338.65	1.32E–04	4.71E–06	2.40E+11	1.06E–03
	22	7	4So 1	2De14	4	4	2.68	4.621	0.00	339.62	1.34E–03	4.74E–05	1.24E+12	1.08E–02
	22	7	4So 1	2De14	4	6	2.68	4.623	0.00	339.79	1.98E–04	7.00E–06	1.23E+11	1.60E–03
	22	7	4So 1	2Pe14	4	4	2.68	4.628	0.00	340.09	1.37E–03	4.84E–05	1.28E+12	1.11E–02
	22	7	4So 1	2Pe14	4	2	2.68	4.628	0.00	340.18	4.43E–08	1.56E–09	8.23E+07	3.57E–07
	22	7	4So 1	2Se14	4	2	2.67	4.640	0.00	341.10	2.19E–04	7.69E–06	4.08E+11	1.76E–03
Total: no. of trans=35							E (keV)=4.604		<f>, < σ_{res} >, <k> =	1.64E+00	1.33E+01	1.67E+05		

Ti ¹⁴⁺ : C _i (1)=1s1s2s2s2p2p2p2p, C _j (18)=1s2s2s2p2p2p2p2p	22	8	3Pe 1	3Po18	5	5	2.710	4.575	0.00	336.29	1.51E–01	6.72E–03	1.37E+14	1.22E+00
	22	8	3Pe 1	3Po18	3	5	2.713	4.570	0.40	336.29	8.86E–02	2.37E–03	4.82E+13	7.14E–01
	22	8	3Pe 1	3Po18	5	3	2.708	4.578	0.00	336.57	5.98E–02	2.67E–03	9.08E+13	4.83E–01
	22	8	3Pe 1	3Po18	3	3	2.711	4.573	0.40	336.57	4.99E–02	1.34E–03	4.53E+13	4.02E–01
	22	8	3Pe 1	3Po18	1	3	2.711	4.573	0.42	336.57	2.12E–01	1.89E–03	6.42E+13	1.71E+00
	22	8	3Pe 1	3Po18	3	1	2.709	4.577	0.40	336.80	7.10E–02	1.90E–03	1.94E+14	5.73E–01
	22	8	1De 1	1Po18	5	3	2.708	4.578	1.06	337.57	2.04E–01	9.11E–03	3.10E+14	1.65E+00
	22	8	1Se 1	1Po18	1	3	2.716	4.565	2.04	337.57	2.13E–01	1.91E–03	6.44E+13	1.72E+00
	22	8	1De 1	3Po18	5	5	2.72	4.562	1.06	336.29	8.88E–03	3.97E–04	8.01E+12	7.16E–02
	22	8	1De 1	3Po18	5	3	2.72	4.565	1.06	336.57	3.63E–03	1.62E–04	5.48E+12	2.93E–02
	22	8	1Se 1	3Po18	1	3	2.72	4.552	2.04	336.57	9.05E–04	8.11E–06	2.71E+11	7.30E–03
	22	8	3Pe 1	1Po18	5	3	2.70	4.594	0.00	337.57	2.56E–03	1.14E–04	3.91E+12	2.07E–02
	22	8	3Pe 1	1Po18	3	3	2.70	4.587	0.40	337.57	3.33E–03	8.88E–05	3.04E+12	2.68E–02
	22	8	3Pe 1	1Po18	1	3	2.70	4.587	0.42	337.57	1.01E–03	9.00E–06	3.08E+11	8.16E–03
Total: no. of trans=14							E (keV)=4.575		<f>, < σ_{res} >, <k> =	1.07E+00	8.63E+00	1.09E+05		
Ti ¹³⁺ : C _i (1)=1s1s2s2s2p2p2p2p2p, C _j (16)=1s2s2s2p2p2p2p2p2p														

Table 2 (continued)

Z	N_e	$SL\pi C_i$	$SL\pi C_j$	g_i	g_j	$\lambda (\text{\AA})$	E (keV)	E_i (Ry)	E_j (Ry)	f_{ij}	S	$A_{ji} (\text{s}^{-1})$	σ_{Pl} (Mb)
22	9	2Po 1	2Se16	4	2	2.729	4.543	0.00	333.94	1.07E-01	3.85E-03	1.92E+14	8.63E-01
22	9	2Po 1	2Se16	2	2	2.733	4.537	0.50	333.94	1.07E-01	1.92E-03	9.55E+13	8.62E-01
Total: no. of trans=2				$E (\text{keV})=4.541$			$\langle f \rangle, \langle \sigma_{\text{res}} \rangle, \langle \kappa \rangle =$			2.14E-01	1.73E+00	2.17E+04	
$\text{Cu}^{28+}: C_i(1)=1s, C_j(3)=2p, E_K \geq 10.85 \text{ keV}$													
29	1	2Se 1	2Po 3	2	2	1.430	8.670	0.00	637.26	1.34E-01	1.26E-03	4.36E+14	1.08E+00
29	1	2Se 1	2Po 3	2	4	1.425	8.701	0.00	639.64	2.66E-01	2.49E-03	4.36E+14	2.14E+00
Total: no. of trans=2				$E (\text{keV})=8.692$			$\langle f \rangle, \langle \sigma_{\text{res}} \rangle, \langle \kappa \rangle =$			3.99E-01	3.22E+00	3.05E+04	
$\text{Cu}^{27+}: C_i(1)=1s1s, C_j(3)=1s2p$													
29	2	1Se 1	1Po 3	1	3	1.475	8.406	0.00	617.62	6.84E-01	3.32E-03	6.99E+14	5.52E+00
29	2	1Se 1	3Po 3	1	3	1.48	8.360	0.00	614.33	8.55E-02	4.18E-04	8.64E+13	6.90E-01
Total: no. of trans=2				$E (\text{keV})=8.403$			$\langle f \rangle, \langle \sigma_{\text{res}} \rangle, \langle \kappa \rangle =$			7.70E-01	6.21E+00	5.88E+04	
$\text{Cu}^{26+}: C_i(1)=1s1s2s, C_j(11)=1s2s2p$													
29	3	2Se 1	2Po11	2	2	1.485	8.349	0.00	613.49	1.33E-01	1.30E-03	4.01E+14	1.07E+00
29	3	2Se 1	2Po11	2	4	1.482	8.366	0.00	614.73	4.74E-01	4.63E-03	7.20E+14	3.82E+00
29	3	2Se 1	2Po11	2	2	1.480	8.377	0.00	615.86	1.13E-01	1.11E-03	3.46E+14	9.15E-01
29	3	2Se 1	2Po11	2	4	1.479	8.383	0.00	616.18	3.69E-04	3.59E-06	5.63E+11	2.98E-03
29	3	2Se 1	4Po11	2	2	1.49	8.299	0.00	610.05	3.27E-03	3.22E-05	9.79E+12	2.64E-02
29	3	2Se 1	4Po11	2	4	1.49	8.310	0.00	610.57	2.41E-02	2.37E-04	3.62E+13	1.95E-01
Total: no. of trans=6				$E (\text{keV})=8.370$			$\langle f \rangle, \langle \sigma_{\text{res}} \rangle, \langle \kappa \rangle =$			7.48E-01	6.03E+00	5.72E+04	
$\text{Cu}^{25+}: C_i(1)=1s1s2s2s, C_j(28)=1s2s2s2p$													
29	4	1Se 1	1Po28	1	3	1.487	8.338	0.00	612.90	6.17E-01	3.02E-03	6.21E+14	4.98E+00
29	4	1Se 1	3Po28	1	3	1.49	8.299	0.00	609.98	7.42E-02	3.65E-04	7.39E+13	5.99E-01
Total: no. of trans=2				$E (\text{keV})=8.339$			$\langle f \rangle, \langle \sigma_{\text{res}} \rangle, \langle \kappa \rangle =$			6.92E-01	5.58E+00	5.29E+04	
$\text{Cu}^{24+}: C_i(1)=1s1s2s2s2p, C_j(23)=1s2s2s2p2p$													
29	5	2Po 1	2Pe23	2	2	1.496	8.288	0.00	609.24	2.52E-01	2.48E-03	7.50E+14	2.03E+00
29	5	2Po 1	2Pe23	4	2	1.500	8.266	1.86	609.24	3.07E-02	6.07E-04	1.82E+14	2.48E-01
29	5	2Po 1	2De23	2	4	1.496	8.288	0.00	609.30	3.07E-01	3.02E-03	4.58E+14	2.48E+00
29	5	2Po 1	2De23	4	4	1.500	8.266	1.86	609.30	2.45E-02	4.84E-04	7.26E+13	1.98E-01
29	5	2Po 1	2De23	4	6	1.498	8.277	1.86	610.24	1.39E-01	2.73E-03	2.75E+14	1.12E+00
29	5	2Po 1	2Pe23	2	4	1.491	8.316	0.00	611.30	5.41E-03	5.31E-05	8.12E+12	4.37E-02
29	5	2Po 1	2Pe23	4	4	1.495	8.293	1.86	611.30	2.83E-01	5.57E-03	8.43E+14	2.28E+00
29	5	2Po 1	2Se23	2	2	1.489	8.327	0.00	612.20	4.26E-04	4.17E-06	1.28E+12	3.43E-03
29	5	2Po 1	2Se23	4	2	1.493	8.304	1.86	612.20	6.50E-02	1.28E-03	3.89E+14	5.24E-01
29	5	2Po 1	4Pe23	2	2	1.50	8.249	0.00	606.21	2.18E-02	2.16E-04	6.44E+13	1.76E-01
29	5	2Po 1	4Pe23	4	2	1.51	8.222	1.86	606.21	1.73E-04	3.43E-06	1.02E+12	1.40E-03
29	5	2Po 1	4Pe23	2	4	1.50	8.260	0.00	607.29	1.20E-04	1.19E-06	1.78E+11	9.70E-04
29	5	2Po 1	4Pe23	4	4	1.50	8.238	1.86	607.29	5.70E-03	1.13E-04	1.68E+13	4.60E-02
29	5	2Po 1	4Pe23	4	6	1.50	8.249	1.86	607.99	3.61E-02	7.15E-04	7.11E+13	2.91E-01
Total: no. of trans=14				$E (\text{keV})=8.287$			$\langle f \rangle, \langle \sigma_{\text{res}} \rangle, \langle \kappa \rangle =$			1.17E+00	9.43E+00	8.94E+04	
$\text{Cu}^{23+}: C_i(1)=1s1s2s2s2p2p, C_j(17)=1s2s2s2p2p2p$													
29	6	3Pe 1	3Do17	1	3	1.503	8.249	0.00	606.13	4.33E-01	2.14E-03	4.26E+14	3.49E+00
29	6	3Pe 1	3Do17	3	3	1.507	8.227	1.32	606.13	2.98E-03	4.43E-05	8.76E+12	2.40E-02
29	6	3Pe 1	3Do17	5	3	1.508	8.222	1.89	606.13	2.43E-02	6.04E-04	1.19E+14	1.96E-01
29	6	3Pe 1	3Do17	3	5	1.506	8.233	1.32	606.52	1.68E-01	2.51E-03	2.97E+14	1.36E+00
29	6	3Pe 1	3Do17	5	5	1.507	8.227	1.89	606.52	2.25E-03	5.58E-05	6.61E+12	1.81E-02
29	6	3Pe 1	3Do17	5	7	1.506	8.233	1.89	607.06	1.02E-01	2.53E-03	2.14E+14	8.22E-01
29	6	3Pe 1	3So17	1	3	1.500	8.266	0.00	607.51	2.37E-02	1.17E-04	2.34E+13	1.91E-01
29	6	3Pe 1	3So17	3	3	1.503	8.249	1.32	607.51	2.22E-01	3.29E-03	6.54E+14	1.79E+00
29	6	3Pe 1	3So17	5	3	1.505	8.238	1.89	607.51	4.96E-02	1.23E-03	2.44E+14	4.00E-01
29	6	1De 1	1Do17	5	5	1.508	8.222	3.67	608.13	5.60E-02	1.39E-03	1.64E+14	4.52E-01

29	6	3Pe 1	3Po17	3	1	1.502	8.255	1.32	608.15	3.74E–02	5.55E–04	3.32E+14	3.02E–01
29	6	3Pe 1	3Po17	1	3	1.497	8.282	0.00	608.53	1.52E–05	7.51E–08	1.51E+10	1.23E–04
29	6	3Pe 1	3Po17	3	3	1.501	8.260	1.32	608.53	4.27E–03	6.33E–05	1.26E+13	3.44E–02
29	6	3Pe 1	3Po17	5	3	1.502	8.255	1.89	608.53	8.46E–02	2.09E–03	4.17E+14	6.82E–01
29	6	3Pe 1	3Po17	3	5	1.498	8.277	1.32	609.62	1.90E–03	2.81E–05	3.39E+12	1.53E–02
29	6	3Pe 1	3Po17	5	5	1.499	8.271	1.89	609.62	2.17E–04	5.37E–06	6.45E+11	1.75E–03
29	6	1De 1	1Po17	5	3	1.502	8.255	3.67	610.55	1.18E–01	2.92E–03	5.82E+14	9.51E–01
29	6	1Se 1	1Po17	1	3	1.505	8.238	4.98	610.55	3.73E–01	1.85E–03	3.66E+14	3.01E+00
29	6	3Pe 1	5So17	3	5	1.51	8.205	1.32	604.21	1.39E–02	2.08E–04	2.44E+13	1.12E–01
29	6	3Pe 1	5So17	5	5	1.51	8.195	1.89	604.21	6.93E–03	1.72E–04	2.02E+13	5.58E–02
29	6	1De 1	5So17	5	5	1.52	8.173	3.67	604.21	2.25E–04	5.62E–06	6.52E+11	1.82E–03
29	6	1De 1	3Do17	5	3	1.51	8.195	3.67	606.13	5.78E–04	1.44E–05	2.81E+12	4.66E–03
29	6	1Se 1	3Do17	1	3	1.52	8.178	4.98	606.13	5.57E–04	2.78E–06	5.39E+11	4.49E–03
29	6	1De 1	3Do17	5	5	1.51	8.200	3.67	606.52	8.54E–03	2.12E–04	2.49E+13	6.89E–02
29	6	1De 1	3Do17	5	7	1.51	8.211	3.67	607.06	5.71E–02	1.42E–03	1.19E+14	4.61E–01
29	6	1De 1	3So17	5	3	1.51	8.216	3.67	607.51	1.74E–02	4.32E–04	8.49E+13	1.40E–01
29	6	1Se 1	3So17	1	3	1.51	8.200	4.98	607.51	5.47E–06	2.72E–08	5.31E+09	4.41E–05
29	6	3Pe 1	1Do17	3	5	1.50	8.255	1.32	608.13	4.70E–03	6.98E–05	8.35E+12	3.79E–02
29	6	3Pe 1	1Do17	5	5	1.50	8.249	1.89	608.13	1.87E–01	4.64E–03	5.53E+14	1.51E+00
29	6	1De 1	3Po17	5	3	1.51	8.227	3.67	608.53	2.82E–03	7.00E–05	1.38E+13	2.28E–02
29	6	1Se 1	3Po17	1	3	1.51	8.211	4.98	608.53	7.95E–02	3.95E–04	7.76E+13	6.41E–01
29	6	1De 1	3Po17	5	5	1.50	8.244	3.67	609.62	1.96E–01	4.86E–03	5.79E+14	1.58E+00
29	6	3Pe 1	1Po17	1	3	1.49	8.304	0.00	610.55	4.90E–04	2.41E–06	4.89E+11	3.95E–03
29	6	3Pe 1	1Po17	3	3	1.50	8.288	1.32	610.55	1.40E–03	2.06E–05	4.16E+12	1.13E–02
29	6	3Pe 1	1Po17	5	3	1.50	8.282	1.89	610.55	4.53E–04	1.12E–05	2.25E+12	3.66E–03

Total: no. of trans=35

 $E \text{ (keV)} = 8.244$ $\langle f \rangle, \langle \sigma_{\text{res}} \rangle, \langle \kappa \rangle =$

2.28E+00

1.84E+01

1.74E+05

 $\text{Cu}^{22+}: C_i(1)=1s1s2s2s2p2p2p, C_j(14)=1s2s2s2p2p2p2p$

29	7	4So 1	4Pe14	4	4	1.512	8.200	0.00	602.80	1.40E–01	2.78E–03	4.08E+14	1.13E+00
29	7	4So 1	4Pe14	4	2	1.511	8.205	0.00	603.07	5.56E–02	1.11E–03	3.25E+14	4.49E–01
29	7	2Do 1	2Pe14	4	4	1.513	8.195	1.63	604.12	2.19E–01	4.36E–03	6.38E+14	1.76E+00
29	7	2Do 1	2Pe14	6	4	1.514	8.189	2.26	604.12	2.94E–02	8.79E–04	1.28E+14	2.37E–01
29	7	2Po 1	2Pe14	2	4	1.516	8.178	3.10	604.12	4.02E–03	4.01E–05	5.83E+12	3.24E–02
29	7	2Po 1	2Pe14	4	4	1.519	8.162	4.32	604.12	7.30E–03	1.46E–04	2.11E+13	5.89E–02
29	7	2Do 1	2Pe14	4	6	1.511	8.205	1.63	604.81	3.48E–03	6.92E–05	6.78E+12	2.81E–02
29	7	2Do 1	2De14	6	6	1.512	8.200	2.26	604.81	1.44E–01	4.31E–03	4.21E+14	1.16E+00
29	7	2Po 1	2De14	4	6	1.518	8.168	4.32	604.81	1.04E–01	2.07E–03	2.00E+14	8.36E–01
29	7	2Do 1	2Pe14	4	2	1.510	8.211	1.63	605.19	7.90E–02	1.57E–03	4.62E+14	6.37E–01
29	7	2Po 1	2Pe14	2	2	1.513	8.195	3.10	605.19	1.70E–01	1.69E–03	4.94E+14	1.37E+00
29	7	2Po 1	2Pe14	4	2	1.517	8.173	4.32	605.19	2.68E–02	5.35E–04	1.56E+14	2.16E–01
29	7	2Do 1	2De14	4	4	1.509	8.216	1.63	605.36	7.56E–04	1.50E–05	2.21E+12	6.10E–03
29	7	2Do 1	2De14	6	4	1.511	8.205	2.26	605.36	1.42E–01	4.23E–03	6.21E+14	1.14E+00
29	7	2Po 1	2De14	2	4	1.513	8.195	3.10	605.36	1.47E–01	1.47E–03	2.15E+14	1.19E+00
29	7	2Po 1	2De14	4	4	1.516	8.178	4.32	605.36	6.17E–02	1.23E–03	1.79E+14	4.97E–01
29	7	2Po 1	2Se14	2	2	1.508	8.222	3.10	607.40	9.85E–04	9.78E–06	2.89E+12	7.94E–03
29	7	2Po 1	2Se14	4	2	1.511	8.205	4.32	607.40	1.37E–01	2.73E–03	8.02E+14	1.11E+00
29	7	2Do 1	4Pe14	4	6	1.52	8.168	1.63	601.85	3.01E–02	6.02E–04	5.81E+13	2.43E–01
29	7	2Do 1	4Pe14	6	6	1.52	8.157	2.26	601.85	1.38E–02	4.15E–04	4.00E+13	1.12E–01
29	7	2Po 1	4Pe14	4	6	1.52	8.130	4.32	601.85	1.47E–04	2.96E–06	2.82E+11	1.19E–03
29	7	2Do 1	4Pe14	4	4	1.52	8.178	1.63	602.80	6.35E–03	1.27E–04	1.84E+13	5.12E–02
29	7	2Do 1	4Pe14	6	4	1.52	8.173	2.26	602.80	1.20E–02	3.59E–04	5.21E+13	9.66E–02
29	7	2Po 1	4Pe14	2	4	1.52	8.157	3.10	602.80	2.63E–04	2.64E–06	3.80E+11	2.12E–03
29	7	2Po 1	4Pe14	4	4	1.52	8.141	4.32	602.80	1.74E–03	3.50E–05	5.02E+12	1.41E–02
29	7	2Do 1	4Pe14	4	2	1.51	8.184	1.63	603.07	1.56E–03	3.11E–05	9.06E+12	1.26E–02

Table 2 (continued)

Z	N_e	$SL\pi C_i$	$SL\pi C_j$	g_i	g_j	$\lambda (\text{\AA})$	E (keV)	$E_i (\text{Ry})$	$E_j (\text{Ry})$	f_{ij}	S	$A_{ji} (\text{s}^{-1})$	$\sigma_{pl} (\text{Mb})$
29	7	2Po 1	4Pe14	2	2	1.52	8.162	3.10	603.07	1.75E-02	1.75E-04	5.06E+13	1.41E-01
29	7	2Po 1	4Pe14	4	2	1.52	8.146	4.32	603.07	2.98E-04	5.98E-06	1.72E+12	2.41E-03
29	7	4So 1	2Pe14	4	4	1.51	8.222	0.00	604.12	7.35E-03	1.46E-04	2.16E+13	5.93E-02
29	7	4So 1	2De14	4	6	1.51	8.227	0.00	604.81	1.61E-04	3.20E-06	3.16E+11	1.30E-03
29	7	4So 1	2Pe14	4	2	1.51	8.233	0.00	605.19	5.27E-04	1.04E-05	3.10E+12	4.25E-03
29	7	4So 1	2De14	4	4	1.50	8.238	0.00	605.36	2.10E-03	4.16E-05	6.18E+12	1.69E-02
29	7	4So 1	2Se14	4	2	1.50	8.266	0.00	607.40	2.28E-04	4.50E-06	1.35E+12	1.84E-03
29	7	2Do 1	2Se14	4	2	1.50	8.244	1.63	607.40	2.13E-04	4.21E-06	1.25E+12	1.71E-03
Total: no. of trans=35		E (keV)=8.193						$\langle f \rangle, \langle \sigma_{\text{res}} \rangle, \langle \kappa \rangle =$		1.70E+00	1.37E+01	1.30E+05	
$\text{Cu}^{21+}: C_i(1)=1s1s2s2s2p2p2p, C_j(14)=1s2s2s2p2p2p2p$													
29	7	4So 1	4Pe14	4	6	1.514	8.189	0.00	601.85	1.32E-01	2.63E-03	2.56E+14	1.06E+00
29	7	4So 1	4Pe14	4	4	1.512	8.200	0.00	602.80	1.40E-01	2.78E-03	4.08E+14	1.13E+00
29	7	4So 1	4Pe14	4	2	1.511	8.205	0.00	603.07	5.56E-02	1.11E-03	3.25E+14	4.49E-01
29	7	2Do 1	2Pe14	4	4	1.513	8.195	1.63	604.12	2.19E-01	4.36E-03	6.38E+14	1.76E+00
29	7	2Do 1	2Pe14	6	4	1.514	8.189	2.26	604.12	2.94E-02	8.79E-04	1.28E+14	2.37E-01
29	7	2Po 1	2Pe14	2	4	1.516	8.178	3.10	604.12	4.02E-03	4.01E-05	5.83E+12	3.24E-02
29	7	2Po 1	2Pe14	4	4	1.519	8.162	4.32	604.12	7.30E-03	1.46E-04	2.11E+13	5.89E-02
29	7	2Do 1	2De14	4	6	1.511	8.205	1.63	604.81	3.48E-03	6.92E-05	6.78E+12	2.81E-02
29	7	2Do 1	2De14	6	6	1.512	8.200	2.26	604.81	1.44E-01	4.31E-03	4.21E+14	1.16E+00
29	7	2Po 1	2De14	4	6	1.518	8.168	4.32	604.81	1.04E-01	2.07E-03	2.00E+14	8.36E-01
29	7	2Do 1	2Pe14	4	2	1.510	8.211	1.63	605.19	7.90E-02	1.57E-03	4.62E+14	6.37E-01
29	7	2Po 1	2Pe14	2	2	1.513	8.195	3.10	605.19	1.70E-01	1.69E-03	4.94E+14	1.37E+00
29	7	2Po 1	2Pe14	4	2	1.517	8.173	4.32	605.19	2.68E-02	5.35E-04	1.56E+14	2.16E-01
29	7	2Do 1	2De14	4	4	1.509	8.216	1.63	605.36	7.56E-04	1.50E-05	2.21E+12	6.10E-03
29	7	2Do 1	2De14	6	4	1.511	8.205	2.26	605.36	1.42E-01	4.23E-03	6.21E+14	1.14E+00
29	7	2Po 1	2De14	2	4	1.513	8.195	3.10	605.36	1.47E-01	1.47E-03	2.15E+14	1.19E+00
29	7	2Po 1	2De14	4	4	1.516	8.178	4.32	605.36	6.17E-02	1.23E-03	1.79E+14	4.97E-01
29	7	2Po 1	2Se14	2	2	1.508	8.222	3.10	607.40	9.85E-04	9.78E-06	2.89E+12	7.94E-03
29	7	2Po 1	2Se14	4	2	1.511	8.205	4.32	607.40	1.37E-01	2.73E-03	8.02E+14	1.11E+00
29	7	2Do 1	4Pe14	4	6	1.52	8.168	1.63	601.85	3.01E-02	6.02E-04	5.81E+13	2.43E-01
29	7	2Do 1	4Pe14	6	6	1.52	8.157	2.26	601.85	1.38E-02	4.15E-04	4.00E+13	1.12E-01
29	7	2Po 1	4Pe14	4	6	1.52	8.130	4.32	601.85	1.47E-04	2.96E-06	2.82E+11	1.19E-03
29	7	2Do 1	4Pe14	4	4	1.52	8.178	1.63	602.80	6.35E-03	1.27E-04	1.84E+13	5.12E-02
29	7	2Do 1	4Pe14	6	4	1.52	8.173	2.26	602.80	1.20E-02	3.59E-04	5.21E+13	9.66E-02
29	7	2Po 1	4Pe14	2	4	1.52	8.157	3.10	602.80	2.63E-04	2.64E-06	3.80E+11	2.12E-03
29	7	2Po 1	4Pe14	4	4	1.52	8.141	4.32	602.80	1.74E-03	3.50E-05	5.02E+12	1.41E-02
29	7	2Do 1	4Pe14	4	2	1.51	8.184	1.63	603.07	1.56E-03	3.11E-05	9.06E+12	1.26E-02
29	7	2Po 1	4Pe14	2	2	1.52	8.162	3.10	603.07	1.75E-02	1.75E-04	5.06E+13	1.41E-01
29	7	2Po 1	4Pe14	4	2	1.52	8.146	4.32	603.07	2.98E-04	5.98E-06	1.72E+12	2.41E-03
29	7	4So 1	2Pe14	4	4	1.51	8.222	0.00	604.12	7.35E-03	1.46E-04	2.16E+13	5.93E-02
29	7	4So 1	2De14	4	6	1.51	8.227	0.00	604.81	1.61E-04	3.20E-06	3.16E+11	1.30E-03
29	7	4So 1	2Pe14	4	2	1.51	8.233	0.00	605.19	5.27E-04	1.04E-05	3.10E+12	4.25E-03
29	7	4So 1	2De14	4	4	1.50	8.238	0.00	605.36	2.10E-03	4.16E-05	6.18E+12	1.69E-02
29	7	4So 1	2Se14	4	2	1.50	8.266	0.00	607.40	2.28E-04	4.50E-06	1.35E+12	1.84E-03
29	7	2Do 1	2Se14	4	2	1.50	8.244	1.63	607.40	2.13E-04	4.21E-06	1.25E+12	1.71E-03
Total: no. of trans=35		E (keV)=8.193						$\langle f \rangle, \langle \sigma_{\text{res}} \rangle, \langle \kappa \rangle =$		1.70E+00	1.37E+01	1.30E+05	
$\text{Cu}^{20+}: C_i(1)=1s1s2s2s2p2p2p2p, C_j(18)=1s2s2s2p2p2p2p2p$													
29	8	3Pe 1	3Po18	5	5	1.521	8.151	0.00	599.31	1.42E-01	3.55E-03	4.09E+14	1.14E+00
29	8	3Pe 1	3Po18	3	5	1.524	8.135	1.50	599.31	9.21E-02	1.39E-03	1.59E+14	7.43E-01
29	8	3Pe 1	3Po18	5	3	1.519	8.162	0.00	599.99	7.79E-02	1.95E-03	3.75E+14	6.28E-01

strengths for the Ti ions lie below the LCLS-XFEL capability of energies up to about 8 keV in the fundamental mode. The XFEL energies may be scanned across the calculated average K_{α} energies for each ion given in Table 2.

Table 2 presents transition parameters and resonant photoionization cross sections (σ_{PI}) for all possible allowed K_α transitions, that is from H- to F-like ionization stages, specified at the top of each set. These resonances lie below the K-shell ionization edge ($1s \rightarrow \infty$ transition) energy E_K , which shifts some to higher energies with increment of the ion charge. E_k is highest for H-like ion. For H-like Al, Ti, and Cu present work includes orbitals up to $4f$ which lies close to but below E_K . For an approximation of E_K , this energy is listed in the title column of each element. Although the transitions correspond to ions, the oscillator strengths and A-values about the same with the additional filled shells, since the charge outside the sphere does not significantly affect the field inside. As stated above, the resonance peaks for each element presented here are higher by orders of magnitude from the background, as well as jump in σ_{PI} at K-shell ionization edge [30]. However, these peaks become weaker with higher excitations, such as K-M, K-N, etc., by ν^{-3} dependence.

Previous works mentioned above [14,15] obtained from Cowan's code compared several approximations from different atomic structure codes and found good agreement within a few percent. Most of the K_{α} transitions are in general strong and hence do not differ due to different approximations. We also find generally good agreement with Palmeri et al. [14] as exemplified in Table 3.

3.1. K_α fluorescence as monochromatic X-ray source

There are several problems in probing the dynamics of inner-shell resonant excitation for practical applications. The extremely high intensities needed to first create and then pump these resonances to appear make it impractical for potential applications, particularly biomedical environments which are unable to withstand such intensities. Although a full-scale model is still to be developed, it is useful to examine some order-of-magnitude estimates, albeit with large uncertainties owing to the vast range of energies and corresponding parameters involved. The typical radiation dose in treatment is generally tolerated for 1 Gray (Gy) = 1 J/kg per minute. 1 Gy is roughly equivalent to approximately 10^{10} photons of 80 keV (gold K-shell ionization energy) irradiated directly at body tissue of area 1 cm². Clearly, such a small dose would be insufficient to drive resonance phenomena that have been observed. Moreover, a monochromatic source is then necessary to scan across the resonance energies. Extremely short pulse time-scales comparable to intrinsic atomic transition rates are required for *in situ* studies of resonant excitation. The femto-second, or shorter, timescales are commensurate with atomic transition rates (Einstein A and B-coefficients), and hence Auger decay radiative cascade rates [6].

These criteria and problems have been addressed by recent XFEL studies. For the low Z atomic species of neon and aluminum, where resonant absorption rates are much smaller than the high Z atoms considered theoretically [2,12], were the focus of the experiments at the SLAC LCLS XFEL [1,6]. Vinko et al. [1] used high intensities,

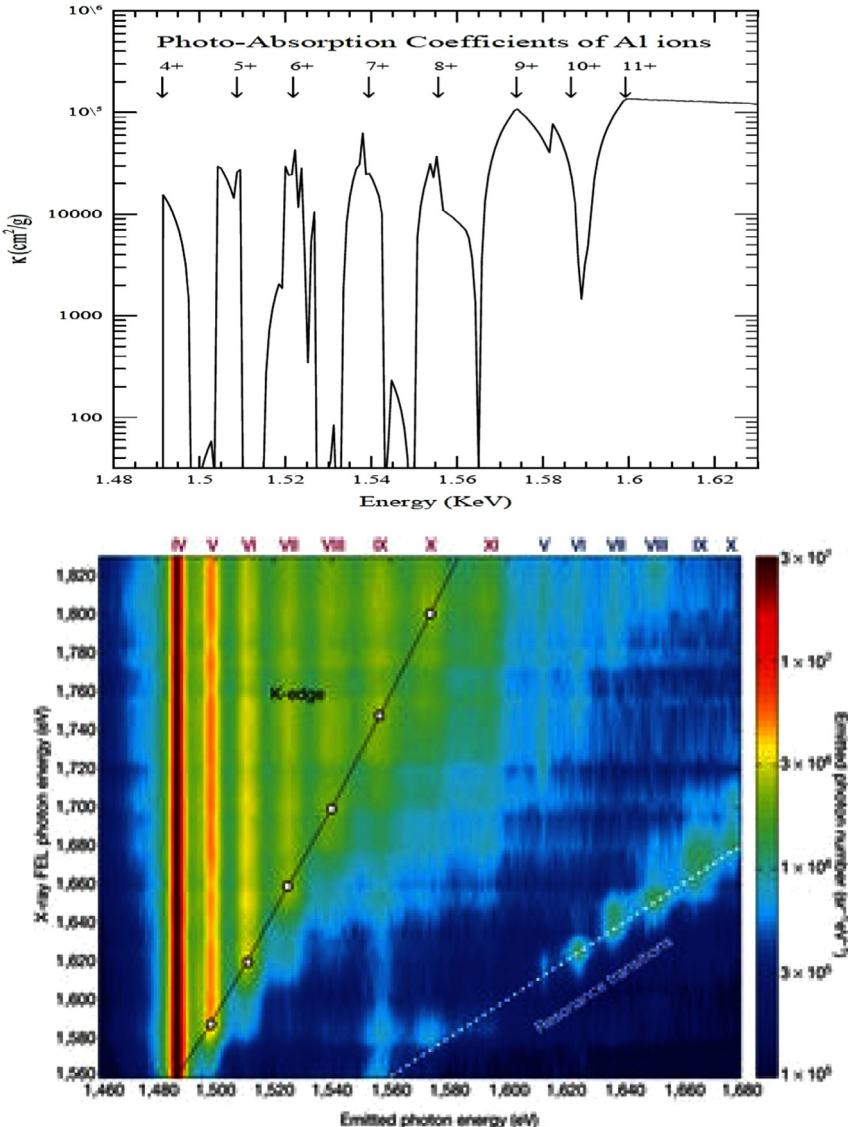


Fig. 3. K_{α} resonance fluorescence in aluminum plasma. Top: theoretically computed K_{α} absorption features in Al ions isoelectronic with fluorine to helium are shown (ionization states are labeled according to ion charge in the upper panel and roman numerals in the lower panel). All contributing K_{α} transition strengths are added together and shown in terms of X-ray attenuation coefficients (cm^2/g) through the Al plasma (convolved over a Gaussian FWHM of 10 eV). Bottom: experimental measurements from the LCLS-XFEL [1] (reproduced with permission). The dashed line on the right shows the resonance transitions with increasing K_{α} emission intensity corresponding to the theoretical absorption complexes. The observed K_{α} features occur when the XFEL energy equals the emitted photon energy.

approximately 10^{17} W/cm^2 , to create and achieve plasma conditions for deep electronic shell vacancies to exist. Given the highly non-linear nature of the dominant terms involved in K_{α} RFL emission, $\sim \Phi^2 \sigma^2 (N_L/A_{pL})$, it should be possible to drive the Auger cycle in Fig. 2 even with the respective resonant cross sections $\sigma_{K\alpha}^R \sim 10^{-18} \text{ cm}^2$ and $\sigma_L(E_{K\alpha}) \sim 10^{-21} \text{ cm}^2$. With minimum Φ_K and $\Phi_{K\alpha}$ fluences of the order of $\sim 10^{20}$ photons/s/cm 2 , one could expect 10^{5-6} K_{α} photons emitted. There is little doubt that the required fluences are available from the LCLS XFEL beams with focused fluence of 10^5 photons per \AA^2 per pulse [7], equivalent to $\sim 10^{33}$ photons/s/cm 2 . It is also likely that they can be attained in synchrotron sources. The important caveat is that a twin-beam set-up is needed, as

proposed in Fig. 2. The isotropic emission of the K_{α} photons should be detectable at an angle away from the directional orientation of incident X-ray beams, in order to avoid swamping the signal by the incident beams or forward scatterings therefrom.

Other monochromatic X-ray sources are being developed using peta-watt (PW) lasers for plasma imaging and K_{α} radiography (e.g. [32–34]). These are also very intense sources, with K_{α} conversion efficiencies of 10^{-4} in the range of laser intensities of $\sim 10^{18-20} \text{ W/cm}^2$. A suitable geometrical arrangement of such sources may also be a viable experimental set-up to drive K_{α} RFL Auger cycle.

A more detailed theoretical and computational formalism than presented herein is needed in order to ascertain

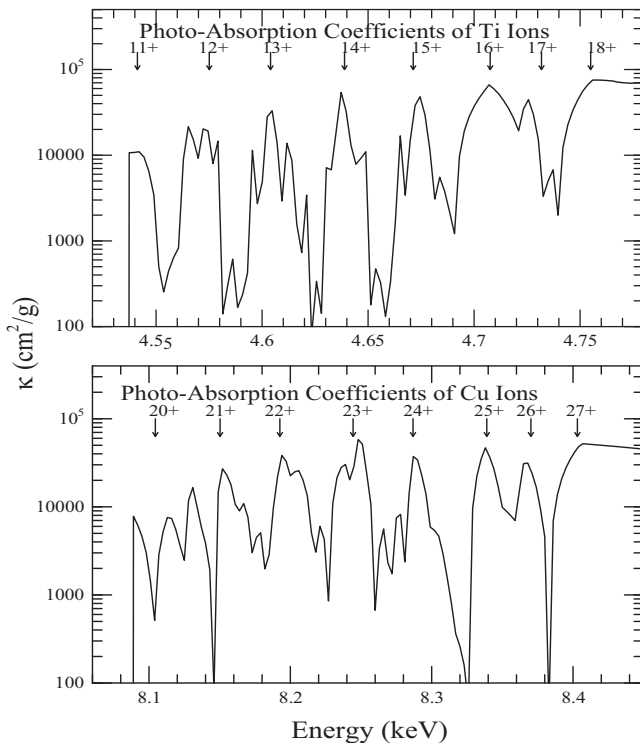


Fig. 4. Ti and Cu K_{α} resonant complexes, as in Fig. 3, in the top and bottom panels respectively. For clarity, the H-like Ti^{19+} and $Cu^{28+} K_{\alpha}$ resonances are omitted since they lie significantly above the He-like Ti^{18+} and Cu^{27+} complexes. The resonance fluorescence of these elements has not yet been observed, but the energies are in the accessible range of beam energies at the LCLS-XFEL.

Table 3

Comparison of the present A -values from SUPERSTRUCTURE (SS) with those from Cown's code by Palmeri et al. [14].

Ion	Transition	A (sec^{-1}) Palmeri et al.	A (sec^{-1}) Present
Al^{+11}	$1s2p^1P_1 - 1s^21S_0$	$2.99E+13$	$2.80E+13$
Al^{+11}	$1s2p^3P_1^o - 1s^21S_0$	$5.61E+10$	$6.26E+10$
Al^{+10}	$1s2s2p^4P_{1/2}^o - 1s^22s^2S_{1/2}$	$4.45E+09$	$4.46E+09$
Al^{+10}	$1s2s2p^4P_{3/2}^o - 1s^22s^2S_{1/2}$	$1.17E+10$	$1.17E+10$
Al^{+10}	$1s2s2p^2P_{1/2}^o - 1s^22s^2S_{1/2}$	$2.43E+13$	$2.25E+13$
Al^{+10}	$1s2s2p^2P_{3/2}^o - 1s^22s^2S_{1/2}$	$2.54E+13$	$2.36E+13$
Al^{+9}	$1s2s^22p^3P_1^o - 1s^22s^21S_0$	$4.01E+10$	$4.38E+10$
Al^{+9}	$1s2s^22p^1P_1^o - 1s^22s^21S_0$	$2.53E+13$	$2.25E+13$

more precisely the incident fluxes needed and K_{α} photons emitted during the resonantly driven Auger cycle. We again note that in addition to the primary physical process of an L-shell vacancy pumped by K-shell photo-excitation, there are several, often competing, processes that need to be accounted for. These include Auger decays and radiative cascades, electron impact ionization dependent on plasma density, and resonance broadening and overlap.

4. Conclusion

Atomic processes related to spectroscopy and transport of K_{α} resonance fluorescence are studied. In particular,

theoretical atomic calculations are carried out with two experimental goals: (i) to elucidate recent observations of XFEL created warm dense matter, and (ii) to introduce a scheme for possible acceleration of Auger decays via twin-beam resonant absorption and resulting fluorescence.

All transition data are available electronically from NORAD-Atomic-Data (NaharOSURadiativeAtomicData) website: http://www.astronomy.ohio-state.edu/~nahar/nahar_radiativeatomicdata/index.html

Acknowledgments

This work was supported partially by NSF AST-1109088 and DOE DE-SC0012331. We would like to thank Sara Lim for comments. The computational work was carried out at the Ohio Supercomputer Center in Columbus Ohio.

References

- [1] Vinko SM, Cricosta O, Cho BI, Engelhorn K, Chung H-K, Brown CRD, et al. Creation and diagnosis of a solid-density plasma with an X-ray free-electron laser. *Nature* 2012;482:59–62;
- [2] Cho BI, Engelhorn K, Vinko SM, Chung H-K, Cricosta O, Rackstraw DS, Falcone RS, et al. Resonant K_{α} Spectroscopy of Solid-Density Aluminum Plasmas. *Phys. Rev. Lett.* 2012;109:245003-1–6.
- [3] Pradhan AK, Nahar SN, Montenegro M, Yu Y, Sur C, Mrozik M, et al. Resonant X-ray enhancement of the auger effect in high-Z atoms, molecules, and nanoparticles: biomedical applications. *J Phys Chem A* 2009;113:12356–63.

- [3] Montenegro M, Nahar SN, Pradhan AK, Yu Y, Huang K. Monte Carlo simulations and atomic calculations for auger processes in biomedical nanotheranostics. *J Phys Chem A* 2009;113:12364–9.
- [4] Nahar SN, Pradhan AK, Montenegro M. Resonant theranostics: a new nano-biotechnological method for cancer treatment using X-ray spectroscopy of nanoparticle. In: Kilho Eom, editor. *Simulations in nanobiotechnology*. New York, USA: CRC Press, Taylor & Francis Group; 2011. p. 305–30.
- [5] Kanter EP, Krissig B, Li Y, March AM, Ho P, Rohringer N, et al. Unveiling and driving hidden resonances with high-fluence, high-intensity X-ray pulses. *Phys Rev Lett* 2011;107:233001-1-5.
- [6] Rohringer N, Ryan D, London RA, Purvis M, Albert F, et al. Atomic inner-shell X-ray laser at 1.46 nanometres pumped by an X-ray free-electron laser. *Nature* 2012;481:488–91.
- [7] Young L, Kanter EP, Krissig B, Li Y, March AM, et al. Femtosecond electronic response of atoms to ultra-intense X-rays. *Nature* 2010;466:56–61.
- [8] Drake RP. *High energy density physics*. Springer Berlin: Springer; 2006.
- [9] Pradhan AK, Chen G-X, Delahaye F, Nahar SN, Oelgoetz J. X-ray resonance opacity of oxygen and iron in AGN MCG-6-30-15. *Mon Not R Astron Soc* 2003;341:1268–71.
- [10] Nahar SN, Pradhan AK, Sur C. Oscillator strengths and radiative transition rates for K_{α} lines in gold X-ray spectra: 1s–2p transitions. *J Quant Spectrosc Radiat Transf* 2008;109:1951–9.
- [11] Sur C, Nahar SN, Pradhan AK. K_{α} transition probabilities for fluorine-like ions from neon to gold: *Ab initio* relativistic coupled-cluster calculations. *Phys Rev A* 2008;77:052502-1-8.
- [12] Nahar SN, Pradhan AK, Lim S. K_{α} transition probabilities for platinum and uranium ions for possible X-ray biomedical applications. *Can J Phys* 2011;89:483–94.
- [13] Nahar SN. X-Rays of heavy elements for nanotechnological applications: W and Pb ions. In: Lotfia El Nadi, editor. *Proceedings of the 4th international conference on modern trends in physics research (MTPR-10)*, Sharm El Sheikh, Egypt; December 12–16, 2010, World Scientific, Singapore, 2013, p. 275–85.
- [14] Palmeri P, Quinet P, Mendoza C, Bautista MA, Garcia J, Witheoft MC, et al. Atomic decay data for modeling the Al K lines. *Astron Astrophys* 2011;525:A59-1-11.
- [15] Palmeri P, Quinet P, Mendoza C, Bautista MA, Garcia J, Witheoft MC, et al. Atomic decay data for modeling K lines of iron peak and light odd-Z elements. *Astron Astrophys* 2012;543:A44-1-9.
- [16] Eissner W, Jones M, Nussbaumer H. Techniques for the calculation of atomic structures and radiative data including relativistic corrections. *Comput Phys Commun* 1974;8:270–306.
- [17] Nahar SN, Eissner W, Chen GX, Pradhan AK. Atomic data from the Iron Project—LIII. Relativistic allowed and forbidden transition probabilities for Fe XVII. *A&A* 2003;408:789–801.
- [18] Elleaume H, Charvet AM, Berkevins P, Berruyer G, Brochard T, et al. Instrumentation of the ESRF medical imaging facility. *Nucl Inst Methods Phys Res A* 1999;428:513–27.
- [19] Kobayashi K, Usami N, Porcel E, Lacombe S, Le Sech C. Enhancement of radiation effects by heavy elements. *Mutat Res* 2010;704:123.
- [20] Lim SN, Pradhan AK, Barth RF, Nahar SN, Nakkula RJ, Yang W, et al. Tumoricidal activity of low-energy 160-KV versus 6-MV X-rays against platinum-sensitized F98 glioma cells. *J Radiat Res*. 2014 (in press, online version: <http://jrr.oxfordjournals.org/content/early/2014/09/28/jrr.084.short?rss=1>).
- [21] Berbeco RI, Ngwa W, Makrigiorgos GM. Localized dose enhancement to tumor blood vessel endothelial cells via megavoltage X-rays and targeted gold nanoparticles: new potential for external beam radiotherapy. *Int J Rad Oncol Biol Phys* 2011;81(1):270276-6.
- [22] Jain S, Coulter JA, Hounsell AR, Butterworth KT, McMahon SJ, et al. Cell-specific radiosensitization by gold nanoparticles at megavoltage radiation energies. *Int J Radiat Oncol Biol Phys* 2011;79(2):531–9.
- [23] Pradhan AK, Nahar SN. Astronomy and cancer research: X-rays and nanotechnology from black holes to cancer therapy. In: Mohan Man, editor. *New trends in atomic and molecular physics advanced technological applications*, 2013. Springer series on atomic, optical, and plasma physics, vol. 76. Berlin, Heidelberg: Springer-Verlag; 2013. p. 253–65.
- [24] Lim S, Montenegro M, Pradhan AK, Nahar SN, Chowdhury E, Yu Y. Broadband and monochromatic X-ray irradiation of platinum: Monte Carlo simulations for dose enhancement factors and resonant theranostics, world congress on medical physics and biomedical engineering. In: Long M, editor. *IFMBE Proceedings* 2012, vol. 39; 2012. Springer, Berlin, p. 2248–51.
- [25] Leung MK, Chow JC, Chithrani BD, Lee MJ, Oms B, Jaffray DA. Irradiation of gold nanoparticles by x-rays, Monte Carlo simulation of dose enhancements and the spatial properties of the secondary electrons production. *Med Phys* 2011;38(2):624–31.
- [26] Yang W, Huo T, Barth RF, Gupta N, Weldon W, et al. Convection enhanced delivery of carboplatin in combination with radiotherapy for the treatment of brain tumors. *J Neurooncol* 2010;101:379–90.
- [27] Lim S, Pradhan AK. Spectral dependence of X-ray radiosensitization with high-Z elements in biological environments; 2014, Under review.
- [28] Pradhan AK, Nahar SN. *Atomic astrophysics and spectroscopy*. Cambridge, UK: Cambridge University Press; 2011.
- [29] International Patent Cooperation Treaty (PCT) Application (pending) WO 2012/054471 A1. Monochromatic X-ray devices and methods of use, The Ohio State University and the Thomas Jefferson University (Anil K. Pradhan and Yan Yu).
- [30] National Institute for Standards and Technology (NIST), X-ray cross section database XCOM at (<http://www.nist.gov/pml/data/xcom/index.cfm>).
- [31] NORAD-Atomic-Data (NaharOSURadiativeAtomicData) website: (www.astronomy.ohio-state.edu/~nahar/nahar_radiativeatomicdata).
- [32] Park HS, Chambers DM, Chung H-K, Clarke RJ, Eagleton R, et al. High-energy K-radiography using high-intensity, short-pulse lasers. *Phys Plasmas* 2006;13:056309-1-10.
- [33] Akli KU, Sanchez del Rio M, Jiang S, Storm MS, Krygier A, et al. A novel zirconium K alpha imager for high energy density physics research. *Rev Sci Instrum* 2011;82:123503-1-6.
- [34] Ovchinnikov VM, Schumacher DW, Kemp GE, Krygier AG, Van Woerkom1 LD, et al. Using time-integrated K images to study refluxing and the extent of pre-plasmas in intense laser-plasma experiment. *Phys Plasmas* 2011;18:112702.